Insights into glacial processes from micromorphology of silt-sized sediment

Allison P. Lepp[1], Lauren E. Miller[1], John B. Anderson[2], Matt O'Regan[3], Monica C.M. Winsborrow[4], James A. Smith[5], Claus-Dieter Hillenbrand[5], Julia S. Wellner[6], Lindsay O. Prothro[7], Evgeny A. Podolskiy[8]

[1]Department of Environmental Sciences, University of Virginia, Charlottesville, VA 22903, USA
[2]Department of Earth Science, Rice University, Houston, TX 77005, USA
[3]Department of Geological Sciences, Stockholm University, 10691 Stockholm, Sweden
[4]iC3: Centre for ice, Cryosphere, Carbon and Climate, Department of Geosciences, UiT the Arctic University of Norway, 9037 Tromsø, Norway
[5] British Antarctic Survey, Natural Environment Research Council, High Cross, Madingley Road, Cambridge, CB3 0ET, UK
[6]Department of Earth and Atmospheric Sciences, University of Houston, Houston, TX 77204, USA
[7]Department of Physical and Environmental Sciences, Texas A&M University - Corpus Christi, Corpus Christi, TX 78412, USA
[8]Arctic Research Center, Hokkaido University, Sapporo, Hokkaido 001-0021, Japan

Correspondence to: Allison P. Lepp (apl2jt@virginia.edu)

Abstract. Meltwater plume deposits (MPDs) from marine sediment cores have elucidated clearly connected, yet difficult to constrain, relationships between ice-marginal landform construction, grounding-zone retreat patterns, and subglacial hydrology for several glacial systems in both hemispheres. Few attempts have been made, however, to infer coveted details of subglacial hydrology, such as flow regime, drainage style, and mode(s) of sediment transport through time from grain-scale characteristics of MPDs. Using MPD, till, and ice-proximal diamicton samples collected offshore of six modern and relict glacial systems in both hemispheres, we examine whether grain-shape distributions and microtexture assemblages (collectively, grain micromorphology) of the silt fraction are the result of subglacial meltwater action, or are indistinguishable from glacial proximal and subglacial sediments from the same region. We find that of all grains imaged (n=9,400), three-quarters can be described by one-quarter of the full range of measured shape morphometrics, indicating widespread and efficient abrasive processes in subglacial environments. Microtexture analysis reveals that while grains comprising MPDs show evidence of edge rounding more often than tills, fluvial microtextures occur in modest amounts on grain surfaces. Furthermore, MPDs retain many mechanical (i.e., glacial) textures in comparable abundances to tills. Significant alteration of MPDs from till sources is observed for systems (1) for which intensive, potentially catastrophic, meltwater drainage events in the Holocene are inferred from marine geologic records, and (2) with comparatively less mature till grains and a contribution of supraglacial melt to the bed, indicating that quantifiable grain-shape alteration of MPDs may reflect a combination of young till, high-energy flow of subglacial meltwater, persistent sediment entrainment, and/or long sediment transport distances. We encourage future works to integrate grain micromorphology into site-specific marine sediment analyses, which may distinguish

periods of persistent, well-connected subglacial discharge from periods of sporadic or disorganized drainage and provide context needed to estimate sediment fluxes and characterize ice response to subglacial meltwater transmission. In addition, this work demonstrates that glacial and fluvial surface textures are retained on silts in adequate abundance for microtexture analysis.

1 Introduction

The distribution and transmission of water beneath ice sheets influences subglacial sediment deformation (Alley et al., 1986; Boulton et al., 2001; Iverson, 2010) and, subsequently, ice-flow dynamics (e.g., Stearns et al., 2008; Gustafson et al., 2022; Livingstone et al., 2022 and references therein). As quantities of ice sheet surface melt production and drainage to the ice sheet bed are modeled to increase in coming decades (Trusel et al., 2015; Lenaerts et al., 2016; Flowers, 2018; Gilbert and Kittel, 2021), continued efforts towards a nuanced understanding of subglacial hydrology at all scales is needed. Marine sediment cores collected from deglaciated continental shelves record discrete meltwater drainage events and persistence of subglacial drainage pathways with temporal resolutions of centuries to millennia (Witus et al., 2014; Prothro et al., 2018; O'Regan et al., 2021; Jennings et al., 2022; Lepp et al., 2022). Numerous marine sediment cores collected offshore of extant continental ice sheets have recovered distinctive meltwater plume deposits (MPDs) that, upon integration into glaciomarine facies models and bathymetric observations, have revealed connections between subglacial hydrologic activity and ice-marginal behavior prior to and during glacial retreat (Simkins et al., 2017; Prothro et al., 2018; O'Regan et al., 2021). However, very little work has been done to infer pertinent details of paleo-subglacial hydrology, such as evolution of drainage pathways or sediment mobilization within subglacial meltwater flow, using subglacially-sourced MPDs.

Research characterizing MPDs has largely relied on grain size (Witus et al., 2014; Simkins et al., 2017; Prothro et al., 2018, 2020), magnetic susceptibility (Witus et al., 2014; Smith et al., 2017), stratigraphy (O'Regan et al., 2021; Lepp et al., 2022; Lešić et al., 2022; Jennings et al., 2022; Clark et al., 2023), and water content (Streuff et al., 2017; Lepp et al., 2022; Clark et al., 2023). In acoustic data, sediments comprising MPDs appear stratified and drape the seafloor topography (Witus et al., 2014; Hogan et al., 2020; Jennings et al., 2022; Lepp et al., 2022; Roseby et al., 2022) reflective of suspension settling, and may infill bathymetric lows or basins (e.g., Nitsche et al., 2013; Witus et al., 2014; Roseby et al., 2022). In sediment cores, MPDs are often laminated or thinly bedded, where subtle variation in grain size between laminae may be indicative of varying plume dynamics, magnitude, or proximity of the ice margin (Ó Cofaigh and Dowdeswell, 2001; O'Regan et al., 2021; Jennings et al., 2022; Lepp et al., 2022; Roseby et al., 2022). Shared grain size modes (Simkins et al., 2017; Prothro et al., 2018), and more recently geochemical similarities (Lepp et al., 2022), between tills, ice-proximal deposits, and MPDs from the same region reflect a common subglacial origin. Furthermore, the grain-size distributions of MPDs collected offshore several Antarctic glacial systems are strikingly similar despite regional variations in subglacial geology (Halberstadt et al., 2016; Simkins et al., 2017; Prothro et al., 2018; Lepp et al., 2022), suggesting the glacial and/or glaciofluvial processes that produce these distinctive sedimentary deposits operate on an ice-sheet scale. The aforementioned processes, however, are poorly

understood and hypothesized mechanisms for subglacial mobilization and sorting of MPDs observed offshore (e.g., Schroeder et al., 2019) have not been empirically evaluated.

70   Grain shape is considered to be a cumulative function of bedrock geology, effects of weathering on preexisting sediments, and sediment transport mechanisms (Mahaney, 2002) and is a powerful proxy for inferring sediment transport history and depositional setting (e.g., Oakey et al., 2005; Campaña et al., 2016; van Hateren et al., 2020), but has been underused in studies that characterize glacial deposits. Of those sparse works, many employ Fourier grain-shape analysis to identify harmonic ranges describing grain elongation, roughness, and transport history (Wellner et al., 2011; Livsey et al.,

75   2013; Witus et al., 2014; Charpentier et al., 2017; Robinson et al., 2021; Clark et al., 2023). In Pine Island Bay, West Antarctica, differences in grain elongation values were calculated between tills and meltwater deposits with even though little variation in grain roughness existed (Witus et al., 2014), providing support for the use of grain shape as an indicator of subglacial sediment transport in glaciomarine environments. Complementary to grain shape, grain microtextures have been more widely examined on glaciogenic grains (Mahaney, 2002; Vos et al., 2014). Suites of microtexture assemblages are associated with different

80   geneses, and have been useful in distinguishing sources of ice-rafted debris (Immonen, 2013; St. John et al., 2015; Passchier et al., 2021), inferring relative ice volume on glacial-interglacial timescales (Cowan et al., 2008), and evaluating distance of proglacial transport (Sweet and Brannan, 2016; Křížek et al., 2017). A micromorphologic (i.e., grain shape and microtexture) approach to examine MPDs and the tills from which they are sourced thus has the potential to reveal process-based details of hydraulic transport and grain-size production in subglacial environments.

85   This study combines a quantitative and qualitative approach to characterize grain micromorphology (encompassing grain shape and microtexture) of MPDs and tills, or ice-proximal diamictons, from six glaciated and formerly glaciated settings in both hemispheres: Ryder Glacier, Thor Iversenbanken, Marguerite Trough, Pine Island Glacier, Thwaites Glacier, and the Ross Sea (Fig. 1). We aim to determine whether MPDs have diagnostic grain-shape distributions and microtexture assemblages and to explore how grain-shape alteration of MPDs from their source materials may record details of subglacial sediment

90   transport and subglacial plumbing through time.

1.1 Bathymetric and glaciological settings of study sites

Ryder Glacier drains from the northwestern Greenland Ice Sheet into the Lincoln Sea through the Sherard Osborn

95   Fjord (O'Regan et al., 2021). Cores sampled for this study were recovered from an along-fjord transect at sites ranging in water depths from 238 m to 633 m (Table A1). Cores from the shallowest water depths (RYDER19-8PC and RYDER19-9PC) were collected atop a prominent bathymetric sill lying close to the modern ice tongue calving line (O'Regan et al., 2021). Glaciomarine sediments derive from both clastic and carbonate sedimentary sources (Henriksen et al., 2009; O'Regan et al., 2021). Early Holocene retreat of Ryder Glacier from the fjord mouth, as well as late Holocene retreat following a glacial

100   readvance, coincide with periods of relatively warm Arctic air temperatures (Levcavalier et al., 2017; O'Regan et al., 2021).

Cores from Thor Iversenbanken in the central Barents Sea were collected from a bathymetric region featuring interconnected basins and channels (Esteves et al., 2022) approximately 15 km from the flow path of the Sentralbankrenna paleo-ice stream (Bjarnadóttir et al., 2014, Esteves et al., 2017). This basin-channel system is interpreted as a series of paleo-subglacial lake basins located beneath non-streaming ice (Esteves et al., 2022), and sedimentological analyses of cores from

105 this region provide evidence for active subglacial drainage between basins (Esteves et al., 2022). The cores included in our study, CAGE-15-5-1221 and CAGE-15-5-1222, were recovered from an adjacent bank area and from within the lower-most basin, respectively (Esteves et al., 2022). Deglaciation of the central Barents Sea is constrained to the late Pleistocene (e.g., Winsborrow et al., 2010). The relict Barents Sea Ice Sheet is heralded as a good analog for the West Antarctic Ice Sheet, due in part to similarities in size and sedimentary subglacial geology (Andreassen and Winsborrow, 2009).

110 The relict Marguerite Trough Ice Stream drained the Antarctic Peninsula Ice Sheet, extending nearly 400 km from the modern coastline to the continental shelf break during the Last Glacial Maximum (LGM; Ó Cofaigh et al., 2014). Geomorphic evidence of ice streaming and a network of channels and remarkably deep (900 m) basins is preserved on the deglaciated continental shelf (Ó Cofaigh et al., 2005; Anderson and Fretwell, 2008; Livingstone et al., 2013). Cores in this study were recovered from within moderately deep basins (Table A1) to the west of George VI Trough (Kennedy and

115 Anderson, 1989). The tills sampled for this study are composed primarily of metamorphic rock fragments and quartz, while the MPDs are rich in silt-sized quartz and feldspar grains (Kennedy and Anderson, 1989). While sediment cores recovered from Marguerite Bay often contain thick units of diatomaceous and organic-rich sediments, the MPD samples in this study were taken from units where siliceous microfossils and organic materials were virtually absent (Kennedy and Anderson, 1989). Initial retreat of the Marguerite Trough Ice Stream occurred coeval with meltwater pulse 1a approximately 14 thousand years

120 (ka) before present (Kilfeather et al., 2011).

Thwaites and Pine Island glaciers drain into the eastern Amundsen Sea Embayment and, during the LGM, coalesced, reaching the outer continental shelf (Kirshner et al., 2012; Larter et al., 2014 and references therein). Retreat across Pine Island Bay initiated during the late Pleistocene and continued in distinct stages until the grounding lines for Pine Island and Thwaites glaciers largely stabilized within ~100 km of their current positions by ~10 ka ago. (Hillenbrand et al., 2013; Nitsche et al.,

125 2013; Witus et al., 2014; Lepp et al., 2022). Cores used in this study (Table A1) were collected on the mid- and inner shelf from a variety of bathymetric settings, including atop an ice-proximal bathymetric high and on a ridge beneath the Pine Island Ice Shelf (Smith et al., 2017). Volcanic and plutonic rocks, largely felsic in composition, underlie the Pine Island and Thwaites glaciers (Smith et al., 2013; Schroeder et al., 2014; Simões Pereira et al., 2020), and large sedimentary basins upstream have been identified by aeromagnetic surveys (e.g., Muto et al., 2016) and inferred by observations of kaolinite-rich sediments

130 offshore (Hillenbrand et al., 2003; Ehrmann et al., 2011; Simões Pereira et al., 2020). Geothermal heat flux is elevated in the region (Damiani et al., 2014; Schroeder et al., 2014; Dziadek et al., 2021).

Cores collected from the western Ross Sea were recovered from bank tops (NBP1502 KC22; Halberstadt et al., 2018) and from topsets and toes of grounding-zone wedges (NBP1502 KC17, KC19; Prothro et al., 2018) in water depths ranging from 354-549 m (Table A1). At the LGM, the East Antarctic Ice Sheet occupied the western Ross Sea (e.g., Anderson et al.,

Figure 1. Graphical map illustrating components of a glacial system that may influence grain-shape alteration and meltwater production compare between study sites. Subglacial geology is binarized into hard (i.e., crystalline) and soft (clastic or carbonate sedimentary) beds. Relict glacial systems and deglaciated setting names are italicized. TI = Thor Iversenbanken, MTIS = Marguerite Trough Ice Stream, PIG = Pine Island Glacier, TG = Thwaites Glacier, Ross = Ross Sea, LGM = Last Glacial Maximum.

135

2014), however, unlike other glacial systems described, landforms on the seafloor indicate that grounded ice did not extend to the continental shelf margin (Greenwood et al., 2012; Halberstadt et al., 2016). High geothermal heat flux is inferred in the western Ross Sea (Simkins et al., 2017) based on the proximity of core sites to volcanic seamounts (Rilling et al., 2009), a rifting zone (Cooper et al., 1987), and measurements (Blackman et al., 1987 and references therein). Tills from this region are composed largely of felsic lithic fragments (Licht et al., 2005).

2 Materials and Methods

A total of 49 sediment samples from MPDs, tills, and ice-proximal glaciomarine diamictons from the regions described in Section 1.1 were gathered for grain-shape analysis (Figure 1; Table A1). For glacial systems from which subglacial till was not available (e.g., Thwaites Glacier), MPD grains were compared directly to ice-proximal diamicton grains. Other

145 systems from which both subglacial till and ice-proximal diamicton were available (e.g., Pine Island Glacier) compared MPD grains against all diamicton grains, merging grains from both till and ice-proximal deposits. While subglacial till and ice-proximal diamicton differ in their depositional environments and processes, the sediment transport processes responsible for grain-shape alteration are largely the same and are distinctly different from sediment transport via subglacial meltwater; therefore, incorporating materials from both subglacial till and ice-proximal diamicton in comparison against MPDs is

150 appropriate to address the goals of this study.

In addition, sediments from basal ice recovered from Siple Dome in the Ross Sea drainage sector of West Antarctica, fringe debris (i.e., sediment entrained into basal ice through infiltration of ice into sediment pore spaces; Rempel, 2008; Meyer et al., 2019) from Pope Glacier in the Amundsen Sea drainage sector of West Antarctica, and supraglacial cryoconite debris from Qaanaaq Glacier in Northwest Greenland, underwent the same suite of analyses and are used to contextualize the

155 micromorphologies observed in our primary sample populations (Table A1).

2.1 Grain-shape analysis

Bulk sediment samples were treated with sodium metaphosphate to deflocculate clays for 48 hours prior to analysis.

160 Tills, ice-proximal diamictons, and basal ice debris were sieved at 500 microns (μm) to isolate matrix material. Cryoconite samples were treated with H_2O_2 to remove organics. Aliquots of sediment from a homogenized slurry were introduced into a Bettersizer S3 Plus sampling reservoir where grain size was measured through laser diffraction. Thousands of images of grains from the same aliquot were subsequently captured using the integrated microscope charge-coupled device camera. Images captured with the 10x objective were exported for shape analysis because this magnification preferentially captures finer grain

165 sizes, including the silt-sized range prevalent in MPDs, than the 0.5x objective. The lower detection limit for the 10x objective is 0.8 μm; to avoid sampling bias skewed towards that threshold or towards clay minerals, images of grains finer than 2.4 μm were excluded from analysis (Crompton et al., 2019).

A MATLAB script for grain-shape analysis (see Data Availability section) randomly selected 200 unique images from each sample, processed images to distinguish foreground from background, converted images from grayscale to binary,

170 and calculated three dimensionless metrics on the binarized shapes using the "regionprops" function (Fig. 2). The metrics considered include eccentricity, circularity, and solidity, and collectively provide information about grain form (i.e., roundness) and shape (regularity). Evaluating distinct shape metrics, rather than harmonic ranges or grain roughness as employed by studies referenced above, allows us to consider the magnitude of variability for each parameter within the context of the other measurements. To test the null hypothesis that grain shapes found in meltwater deposits and subglacial/ice-proximal

175 diamictons from the same glacial systems are indistinguishable, we performed a two-type Z-test on the means of each group for each shape metric considered (probability $p < 0.05$). We calculate 95 % confidence intervals from 1,000 bootstrap replicates for those samples and metrics showing statistically significant differences in means.
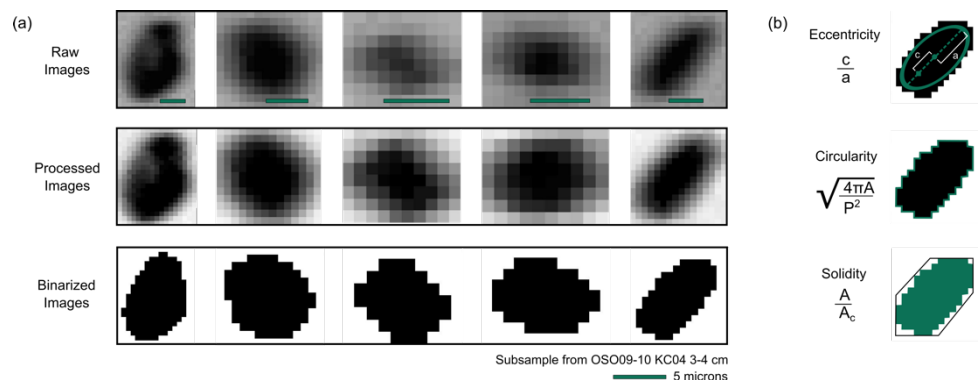
Figure 2. Workflow for automated grain shape analysis. (a) Raw images captured by the Bettersizer S3 Plus, images post-processing, and in binarized forms. (b) Metrics and associated equations calculated for each grain. c = distance between ellipse foci and center; a = length of semi-major axis; A = area, P = perimeter, A_c = area of the convex hull that encompasses the grain.

2.2 Microtexture analysis

Based on the quantitative grain shape output, a subset of samples was imaged by a scanning electron microscope (SEM) for microtexture analysis. An aliquot of the deflocculated sample was pipetted from a homogenized slurry and dispensed onto a 63 µm sieve, where a fraction that passed through was collected onto a piece of weigh paper. Once dried, a section of the weigh paper was mounted, sputter coated (Au-Pd), and imaged using an FEI Quanta 650 field-emission gun in high vacuum mode. Grain composition was verified as quartz through the Oxford AZtec energy dispersive x-ray spectrometer (EDS) program prior to imaging.

Grains were categorized by relief (high to low, following Mahaney, 2002) and roundness (angular to rounded, after Vos et al., 2014). Presence or absence of a suite of microtextures associated with glacial transport (cf. Passchier et al., 2021) and fluvial environments (cf. Vos et al., 2014; Křížek et al., 2017) were identified and calculated in frequency of occurrence (%) for each sample (Fig. 3). Percent overrepresentation is calculated as the difference between mean frequencies of occurrence by sample type for each texture. Microtexture identification primarily followed Mahaney (2002), yet because this canonical reference focuses on the sand fraction, textures on some grains were counted based on appearance rather than the specified scale. For example, Mahaney (2002) specifies arcuate and straight steps occur on the >5 µm scale, while we observed this feature on finer scales (Fig. 3).

3 Results

3.1 Grain-shape distributions of MPDs and tills

Of the metrics considered, eccentricity shows the greatest statistical variance between glacial systems, with standard deviations of 3.4 % and 4 % between medians of all MPD and till or ice-proximal diamicton samples, respectively. Grains from the Marguerite Trough Ice Stream encompass the widest spread of eccentricities for all regions considered, with an average interquartile range of 0.25. Thor Iversenbanken and Marguerite Trough samples contain grains that are generally more eccentric relative to the other four systems. Of those other four systems, Ryder Glacier, Thwaites Glacier, Pine Island Glacier,
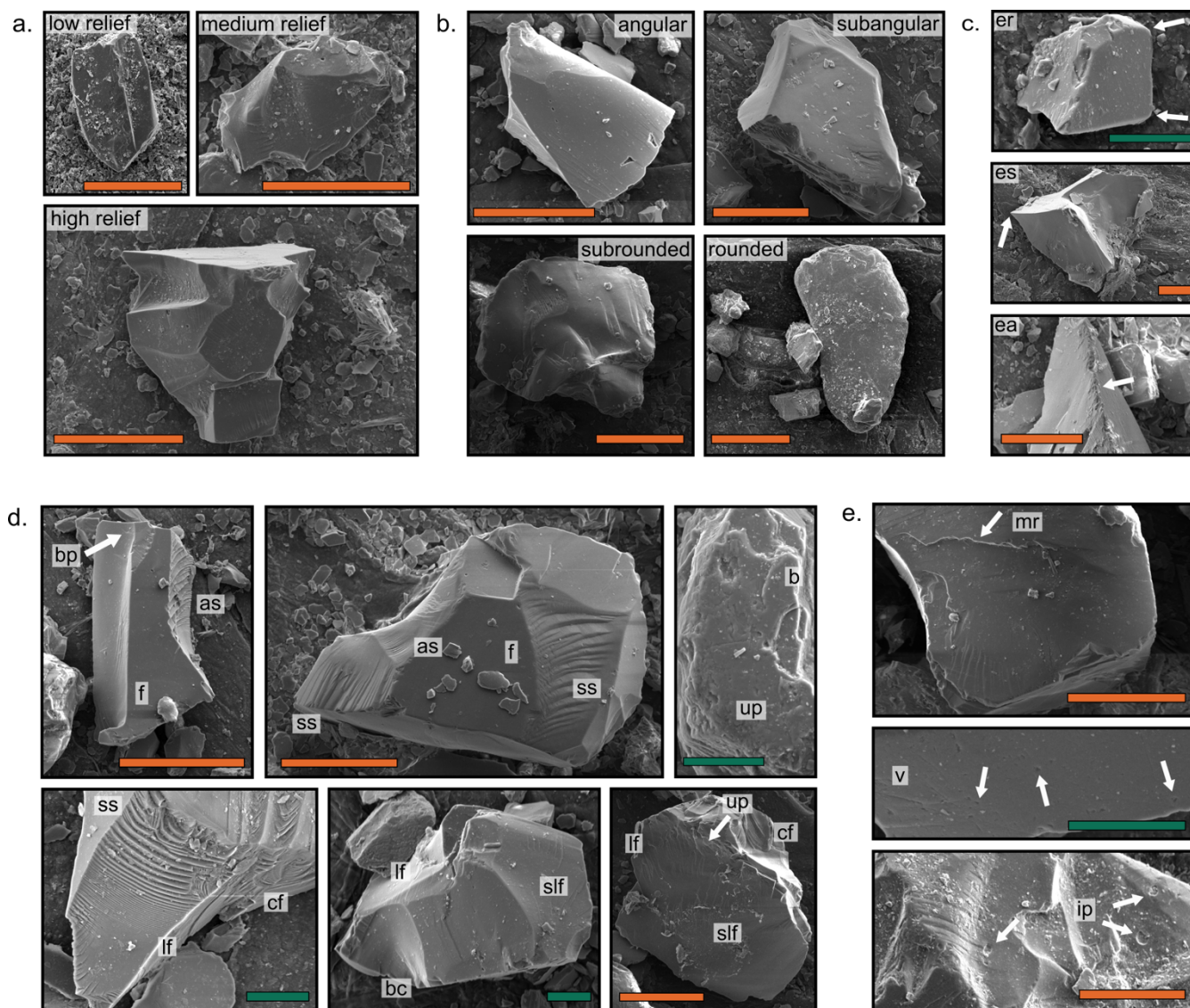
Figure 3. Microtextures observed on quartz grains in the <63 µm size fraction (silt) from select till and meltwater plume deposit samples. Orange scale bar = 20 µm. Green scale bar = 5 µm. (a) Grain relief and (b) grain shape, following Mahaney (2002) and Vos et al. (2014), respectively. (c) Edge characteristics. (d) Fracture types characteristic of glacial transport, following grain types B-D from Passchier et al. (2021). Note the differences in scale bars. (e) Microtextures associated with fluvial transport, following Křížek et al. (2017). as = arcuate steps, b = breakage block, bc = breakage concavity, bp = broken plates, cf = conchoidal fracture, ea = edge abrasion, er = rounded edges, es = sharp edges, f = fracture face, ip = impact pit, lf = linear fracture, mr = meandering ridges, slf = sublinear fracture, ss = straight steps, up = upturned plates, v = v-shaped percussions.

and Ross Sea, distributions of grain eccentricity are strikingly similar with interquartile ranges from 0.38 to 0.66 for both grain populations (Fig. 4), though the median eccentricity for Thwaites Glacier grains is slightly elevated at 0.53. Marguerite Trough

205 Ice Stream is the only system where eccentricities of MPD and till grains are highly significantly different, reflecting MPD grains that are notably less elongate compared to their source material. Eccentricity of MPD and till grains from Pine Island Glacier were determined to be significantly different, again with MPD grains being less elongate (Table A2).

On average, the most circular grains are found in Ross Sea MPDs (mean: 0.63, median: 0.64)
210 while the least circular grains are found in tills from the Thor Iversenbanken (mean: 0.55, median: 0.56). The median circularity of MPD grains is higher compared to tills for all six systems, but differences in means are statistically significant only for Ryder
215 Glacier, Pine Island Glacier, and Ross Sea samples (Fig. 4). Interestingly, interquartile ranges for MPDs from Marguerite Trough Ice Stream and Thwaites Glacier do not show enhanced circularity relative to source material. Instead, compared to their respective
220 source populations, these MPDs appear to have restricted subsets of circularities with similar medians as their corresponding till samples. An intercomparison of MPDs from all systems, with the addition of plume deposits from three systems with no
225 till counterparts, reveals modest variability between interquartile range for all MPDs (0.51-0.69) with no clear regional trend (Fig. 5). MPDs from Marguerite Trough are less circular than other Antarctic deposits and have interquartile ranges very similar to those
230 samples from the Barents Sea (Thor Iversenbanken and Kveithola) and the Nares Ice Stream. Ryder Glacier and Petermann Ice Stream MPDs have the widest interquartile ranges with median values similar to samples from PIG and the Ross Sea,
235 respectively. Some regional differences in circularity, like in NW Greenland where glaciers have similar catchment areas and meltwater sources (Figs. 1, 5), likely reflect varied mineralogy: Petermann Glacier detritus is higher in calcite and dolomite (Jennings et al.,
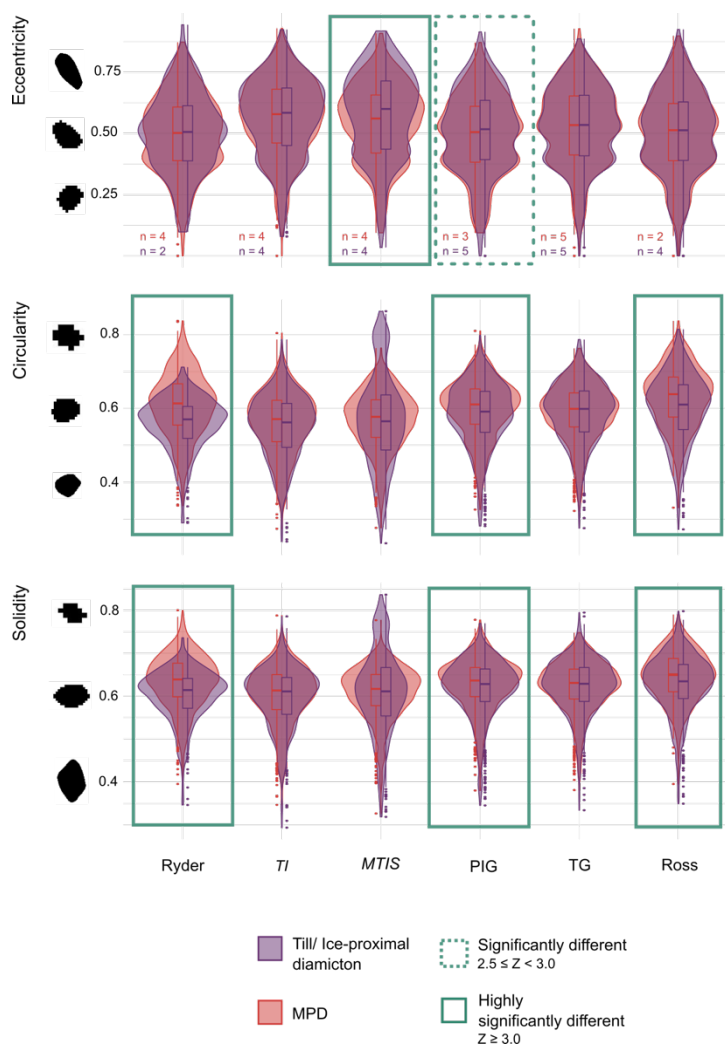
Figure 4. Violin plots for paired MPDs and tills, or ice-proximal diamictons (Table A1), for each region with the number of samples from each grain type shown at the bottom of grain eccentricity. Box plots within each violin show the interquartile ranges. Those pairs outlined in solid green denote populations that are highly significantly different, while the dashed green line indicates pairs that are significantly different as determined by a two-type Z test. Refer to Fig. 2 for shape metric equations. TI = Thor Iversenbanken; MTIS = Marguerite Trough Ice Stream, PIG = Pine Island Glacier, TG = Thwaites Glacier, Ross = Ross Sea.
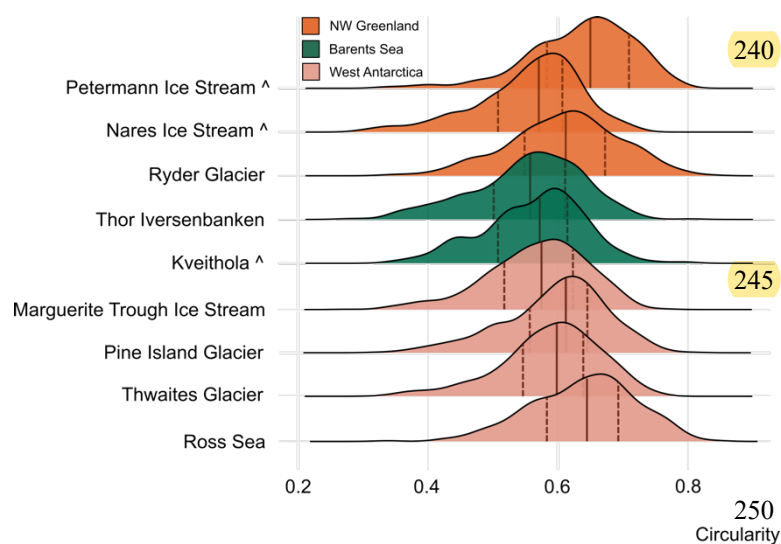
Figure 5. Circularity of meltwater plume deposit grains with first and third quartiles indicated by dashed lines and the median by a solid line. Glacial systems are grouped and colored by region. Samples with no till counterpart are denoted by ^ (see also Table A1).

2022), Nares Ice Stream detritus in quartz and micas (Jennings et al., 2022), while Ryder Glacier detritus consists of both carbonate and clastic sedimentary materials (O'Regan et al., 2021) and shows an interquartile range of grain circularity between the other two. Yet, NW Greenland MPDs have similar distributions of grain circularity to West Antarctica MPDs (Fig. 5) and Ryder Glacier tills are more irregular than West Antarctic tills (Fig. 4), alluding to impacts on MPD grain shape unrelated to source geology. We also note that the circularity distributions for MPDs from all systems overlap with one another and are largely confined between values of 0.4 and 0.8 (Fig. 5).

Solidity describes regularity of grain perimeters, and the interquartile ranges for Ryder Glacier, Thor Iversenbanken, Pine Island Glacier, and the Ross Sea demonstrate shifts to enhanced grain regularity from tills to MPDs, with highly statistically significant differences for all but the Thor Iversenbanken (Fig. 4). As with circularity, MPD grains from Marguerite Trough and Thwaites Glacier exhibit a narrower interquartile range of solidities than is found in corresponding till samples; the mean and median distribution for each grain population is virtually the same for these systems. The median solidity for tills from Ryder Glacier, Thor Iversenbanken, and Marguerite Trough is all 0.61, while those from Pine Island Glacier, Thwaites Glacier, and the Ross Sea are slightly higher (0.628-0.634).

We acknowledge that grain size, and therefore image resolution (Fig. 2), may have some influence on the observed grain-shape distributions. However, none of the distributions for any metric considered are strongly skewed towards upper or lower limits as we would expect if image resolution were controlling the distribution of shape values. These results suggest that the preventative measures integrated into the methodology (removing grains below 2.4 µm; random selection of grains to use in analysis) sufficiently removed any grain-size bias from the quantitative grain-shape results.

3.2 Microtexture observations

A total of 132 grains were imaged from four MPDs and four tills/ice-proximal diamicton (Table A1). Imaging was attempted on approximately twice that number of samples, however the fine-grained and electrostatic nature of MPDs presented challenges in isolating quartz grains in the silt fraction, and many samples imaged were dominated by clays and had fewer than 10 quartz grains. The eight samples included in microtexture observations imaged between 12 and 20 quartz grains, which is within the range considered to be representative for any given SEM sample (cf. Vos et al., 2014).

We observe suites of microtextures characteristic of glacial transport on quartz grains at the micron to sub-micron scale (e.g., Fig. 3d) in both till and MPD populations, indicating microtexture analysis on glaciogenic silts is both feasible and results in meaningful data. Angular grains and grains with high relief are found to be overrepresented in till samples compared to MPDs by 31 % and 10 %, respectively (Fig. 6). Conversely, grains with subangular and subrounded shape, as well as low relief grains, occur in higher abundance in MPDs (Fig. 6). Round grains are comparably rare in till and MPD samples, and grains with medium relief are the most abundant relief type in both sample populations (Fig. 6). All step and fracture textures that are attributed to high stress, grinding, plucking, and abrasion in glacial environments (Vos et al., 2014; Passchier et al., 2021) are overrepresented in till grains, ranging from 3 % (sawtooth fractures) to 18 % (straight steps) more common than in MPDs (Fig. 6). Additionally, breakage features including blocks, concavities, and plates are observed in moderate (≤ 50 %) abundance in both grain types and are largely overrepresented in tills.

Fluvial microtextures imparted to grain surfaces through intergranular collisions during transport in suspension are observed on both till and MPD grains, but with abundances ≤ 25 % are not pervasive features. V-shaped percussion cracks and impact pits are overrepresented in MPD grains by only 5 % and 2 %, respectively, while meandering ridges are, somewhat surprisingly, overrepresented in till/ice-proximal diamicton grains by 4 %. Notably, grains in MPDs exhibit edge rounding 26 % more often than is observed in till and ice-proximal diamicton samples. It is important to note that, while differences in average frequencies allow us to compare microtexture abundance between tills and MPDs, nearly all textures are observed in some abundance in both populations. In other words, overrepresentation of a suite of textures in one grain type does not reflect absence, or even low abundance, of that feature in the other grain type. Edge abrasion and linear fractures, for example, are both overrepresented in till grains, but are seen on over 50 % of grains in both populations.

4 Discussion

We find that quantifiable, significant differences in grain shape exist between MPDs and tills in some regions, as well as between MPDs from different regions, and that those differences can be both quantified using an automated imaging approach and, generally, verified qualitatively with microscopy. Here, we consider potential reasons for those variations and discuss implications for subglacial sediment transport processes, with an emphasis on subglacial hydrology.

4.1 Widespread subglacial sediment transport processes

Despite the variation in subglacial lithology, catchment size, glacial histories, and source(s) of basal meltwater for the glacial systems considered (Fig. 1), we find that three-quarters of all grains studied can be described by approximately one-quarter of possible grain morphologies, alluding to highly efficient and ubiquitous erosive processes that likely operate on catchment-wide scales. Through these processes, grains with extreme morphometries (i.e., highly elongated/rounded, or highly irregular/regular) are either not produced in abundance or such extremes are short-lived. Variability between glacial systems likely reflects differences in regional substrate geology and mineralogy, glacial history (i.e., textural maturity of sediments), distance of transport, volume of meltwater present, or some combination of those factors (Fig. 1). If regional geological and

mineralogical variability were driving differences in grain shape distributions, it is likely that would manifest most clearly in

305   eccentricity because this metric could capture relative proportions of equant and elongated or platy minerals (e.g., Marsaglia et al., 2013). Yet, median eccentricity for all MPD grains varies by only ~8 % between systems (Fig. 4), suggesting geological differences do not fully explain all variation in the dataset. Additionally, no distinctive grain-shape populations emerge that separate (predominately) hard bed from soft bed systems (Fig. 1), further implying that source material alone does not explain
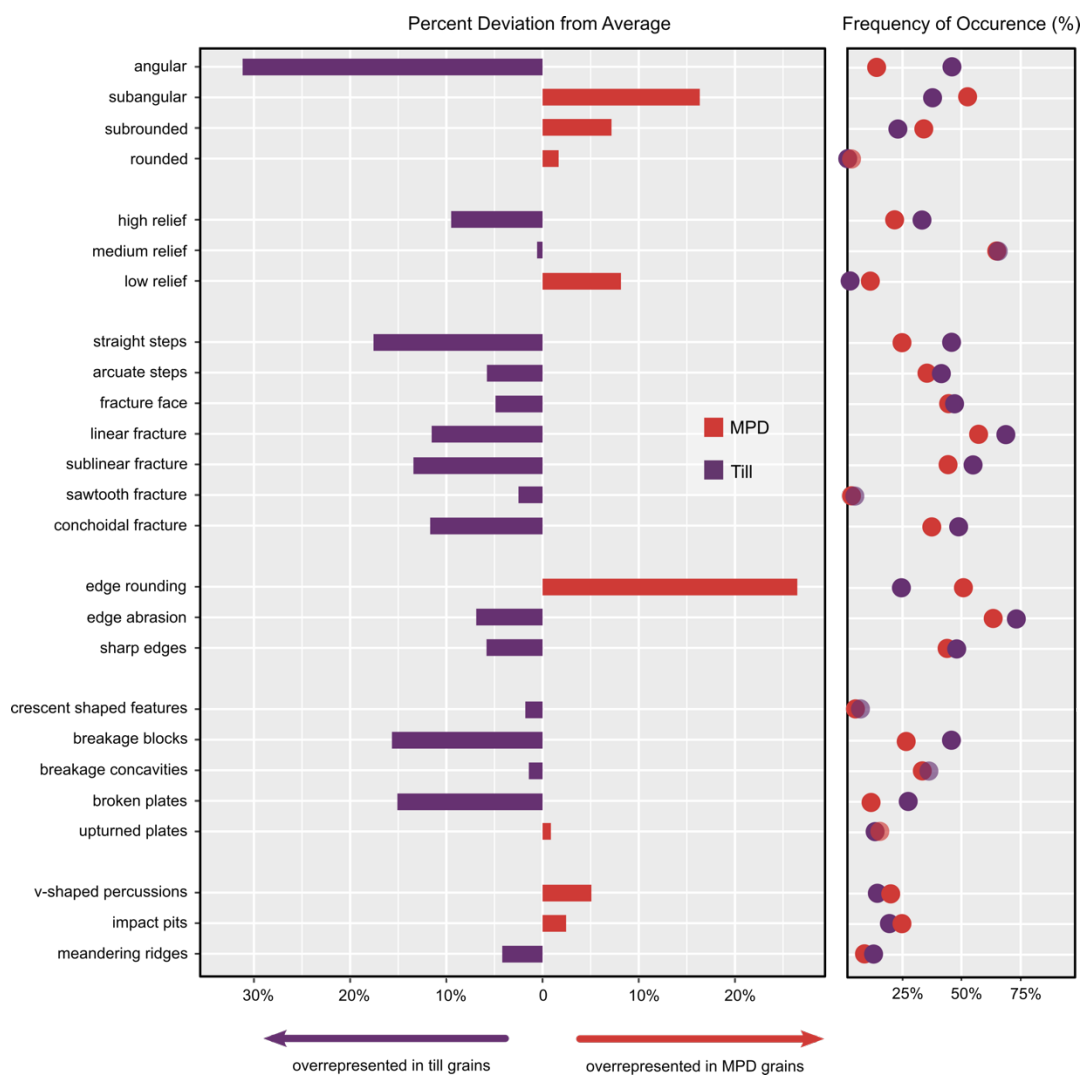
Figure 6. Overrepresentation and frequency of occurrence of microtextures in both grain populations observed on 132 quartz grains. Refer to Fig. 3 for examples of microtextures. Angular grains and all fracture types, as well as edge abrasion, are overrepresented in till grains, whereas MPDs exhibit a higher proportion of subangular and subrounded grains with edge rounding. Many mechanical microtextures (e.g., fracture faces, linear and sublinear fractures) are observed at comparable frequencies in both grain populations.

the minor intrasystem variance.

310   When we consider the shape distributions for supraglacial debris, basal ice debris, and basal fringe debris in relation to tills and MPDs from those regions, the erosive power of subglacial sediment transport becomes abundantly clear (Fig. 7).
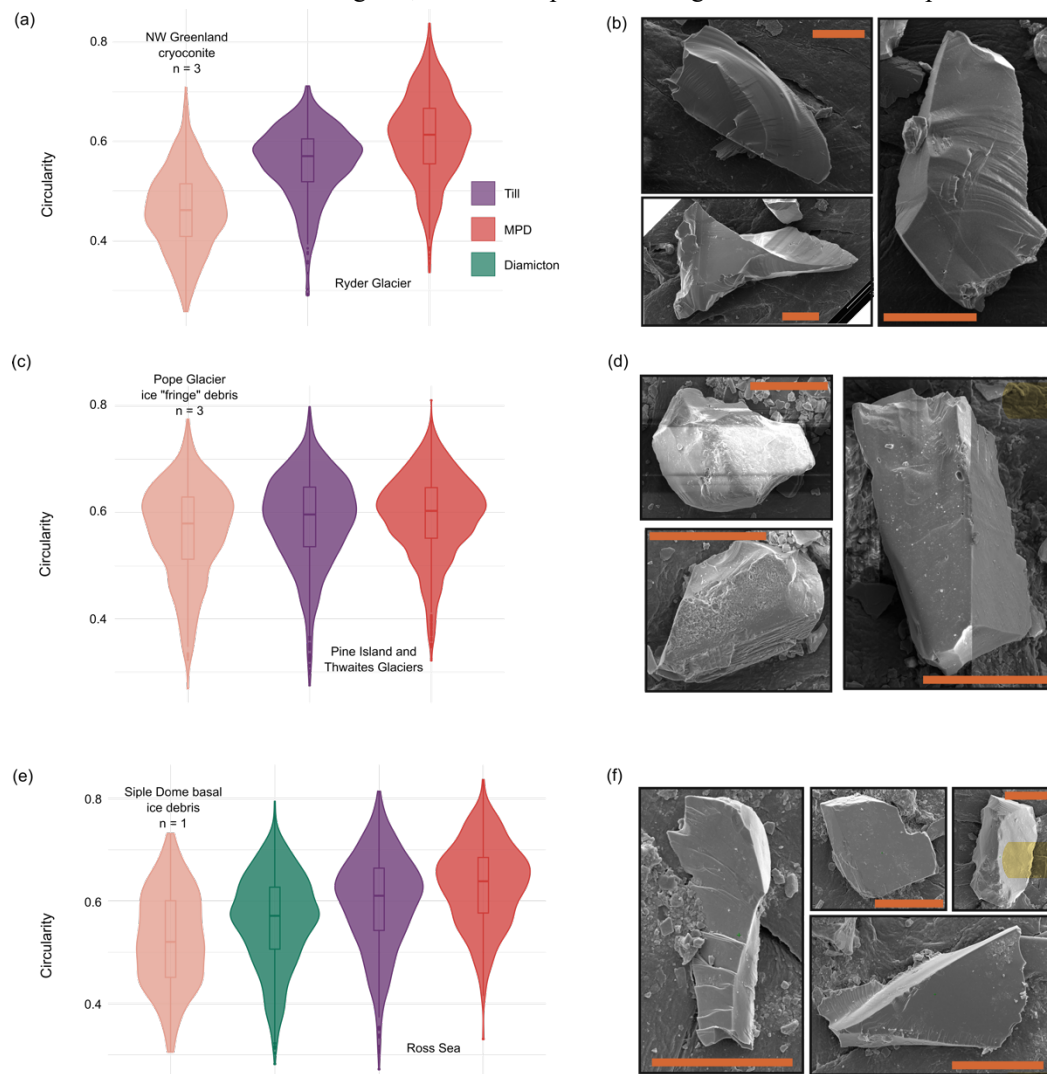
Circularity of cryoconite grains from Qaanaaq Glacier, NW Greenland, and basal ice debris from Siple Dome, West Antarctica, is highly significantly different (Z >> 3.0) from grain circularity of tills recovered from nearby glacial systems. Consistent with microtexture observations (Mahaney, 2002; Cowan et al., 2008), our results suggest that englacial transport minimally influences grain shape and that elongated grains introduced to the till column from basal ice (Fig. 7b) are not

335 preserved in abundance. Supraglacial debris contains grains with markedly different morphology than grains which have been altered in the subglacial

Figure 7. Visualization of grain shape evolution. (a), (c), and (e) show grain circularity for supra- or englacial reference material in comparison to glacial-marine diamicton, till, and meltwater plume deposits from a neighboring glacial system. SEM images of (b) cryoconite, (d) basal fringe debris, and (f) basal ice debris show highly fractured and elongated grains that are less common following subglacial transport. Note that in (c) the middle violin includes samples from ice-proximal diamicton from offshore Pine Island and Thwaites glaciers, as well as subglacial till samples from Pine Island Glacier (Table A1). Scale bar in (b), (d), and (f) is 20 microns.

environment (Fig. 7a). Less pronounced alteration is observed between grains from "dirty ice" of Kay Peak, Pope Glacier and those tills and ice-proximal diamictons in the eastern Amundsen Sea (Thwaites and Pine Island glaciers; Fig. 7c, d).

345   Sediment entrainment, transport, and release from the ice fringe depends on the thermal and pressure conditions of basal ice (Rempel, 2008; Iverson et al., 2017) and is, therefore, spatiotemporally transient in nature. It logically follows that differences in grain circularity are more pronounced between till and basal ice debris or cryoconite grains than between till and fringe debris, because the latter has likely undergone transport processes at the ice-bed interface prior to fringe entrainment. In the Ross Sea, a clear grain-shape continuum emerges from basal ice debris, ice-proximal diamicton, subglacial till, and MPDs where interquartile ranges incrementally shift towards higher abundance of circular grains (Fig. 7e). The intermediate

350   grain characteristics implied within glacial-marine diamicton samples likely reflect inclusion of till pellets (Domack et al., 1999; Cowan et al., 2012; Prothro et al., 2018; Robinson et al., 2021) from basal ice into ice-marginal or gravity flow deposits. The differences we see between MPDs and till sources are more subtle than those between tills and basal ice debris, with the exception of Ryder Glacier (discussed in more detail in the next section).

The added context gleaned from supra- and englacial grain micromorphology indicates that all MPD, till, and

355   diamicton grains in this study experienced alteration through subglacial sediment transport processes, like grain rotation and grinding, that occur predominantly in dilatant, deforming tills (Evans et al., 2006; Robinson et al., 2021). Such tills are associated with high basal water pressures and streaming of glacial ice (e.g., Boulton et al., 2001; Evans et al., 2005; Reinardy et al., 2011; Rüther et al., 2012). Thus, this finding suggests most grains experienced some degree of transport and alteration beneath fast-flowing ice, i.e. conditions that were also inferred from other paleo-subglacial records, such as subglacial

360   bedforms and till properties, in the studied regions (Nitsche et al., 2013; Esteves et al., 2017; Jakobsson et al., 2018; Munoz and Wellner, 2018; Simkins et al., 2018; Kirkham et al., 2019, 2020; Hogan et al., 2022). No geomorphic evidence of ice streaming exists on Thor Iversenbanken (Esteves et al., 2022), however, and sediment grains from this area may have experienced morphological alteration through shearing or brittle deformation (e.g., Evans et al., 2006) that produced a slightly more irregular, elongate shape signature (Fig. 4).

365   The general homogeneity in grain morphology we observe may reflect the lasting impact of grain cushioning, whereby fines fill interstitial spaces between larger till clasts and, through grain rolling, act to absorb and dissipate tensile stresses along grain bridges (Iverson et al., 1996; Menzies, 2012; Robinson et al., 2021). This effect has been shown to produce a self-similar grain-size distribution (Iverson et al., 1996), and it is possible the same may be true for grain shape. While the volume of subglacial meltwater influences how grains through a till column will be mobilized and therefore indirectly affects grain-shape

370   alteration through the processes discussed above, our data suggest subglacial sediment transport is chiefly responsible for producing the largely homogenized grain shape distributions we observe. We acknowledge, of course, the Sisyphean challenges associated with untangling inherited grain shape from earlier glacial cycles or interglacial subaerial sediment transport (Evans et al., 2006), but do not think our inability to do so detracts from the findings of near grain-shape homogeneity in tills and MPD silts from a geographically-diverse sample population.

4.2 Production of meltwater silts

Subglacial processes responsible for generating glacial silts and the "terminal grain-size mode", or the smallest size to which a grain can be comminuted based on its mineralogical structure, have been explored through field observations and controlled experiments (e.g., Dreimanis and Vagners, 1971, 1972; Iverson et al., 1996; Crompton et al., 2019). Those works have largely converged on abrasion as a widespread, dominant process in subglacial environments (Alley et al., 2019) that drives comminution by exploiting weaknesses in the mineral fabric of larger grains (Haldorsen, 1981; Crompton et al., 2019), and the microtextural signatures of abrasion on grain surfaces include different step and fracture types (e.g., Mahaney, 2002; Passchier et al., 2021). Furthermore, abrasion beneath glacial ice has been credited with rounding grain shape (Hart, 2006; Rose and Hart, 2008), which is consistent with the degrees of solidity and circularity in our results, particularly for those most mature (i.e., undergone reworking by multiple glacial advance and retreat cycles) sediments from West Antarctica (Figs. 4, 5).

We observe microtextures resulting from abrasive processes, including conchoidal fractures, arcuate and straight steps, parallel and sub-parallel fractures, on a large proportion of grains from both MPD and till samples (Fig. 6). The abundance of fracture types, edge abrasion, and other microtextures imparted through sustained stress and grinding in addition to the low occurrence of v-shaped percussions on both grain populations strongly suggests the grain-size production of the ~10 µm meltwater-silt mode results from abrasion and grinding at the base of glacial ice, rather than the comminution of grains during subglacial hydrologic transport (e.g., Schroeder et al., 2019). Witus et al. (2014) reached a similar conclusion after examining sand microtextures from MPDs and tills collected offshore PIG (material which we also include in this study, Table A1). Collectively, our results provide grain-scale evidence supporting an inferred subglacial origin for MPDs based on shared grain-size modes (Witus et al., 2014; Simkins et al., 2017; Prothro et al., 2018) and geochemical similarities (Lepp et al., 2022) with till and ice-proximal diamicton.

Although we did not include samples from each study region due to methodological challenges (e.g., insufficient number of quartz grains present on sample stub, adhering particles obscuring quartz grain surfaces), we have found meaningful results from the data subset and have conducted what we believe to be the first quartz microtextural analysis on the silt grain-size fraction. In addition to mechanical textures that offer insight into subglacial sediment transport, we also observed silt grains that retained pre-weathered surfaces and showed signs of silica dissolution. We encourage future microtextural investigations inclusive of, or focused on, the silt fraction because of the additional context those grains may hold for glacial histories, sediment transport processes, or paleoclimate reconstructions of glaciated or formerly glaciated regions.

4.3 Subglacial hydrological inferences from grain micromorphology

While we do not observe homogeneity in grain-shape distributions of MPDs as striking as is seen with grain size (e.g., Witus et al., 2014; Prothro et al., 2018; Jennings et al., 2022; Lepp et al., 2022), we do find that median circularity (Fig. 5) and eccentricity of all MPDs in this study vary by less than 10 % and that distributions overlap with one another; however,

because shape distributions also overlap with till and ice-proximal diamicton grains, we cannot describe the MPD grain-shape distributions as diagnostic. Similarly, we do not observe pervasive evidence of glaciofluvial transport in surface microtextures on MPDs (Fig. 6). These deposits are described as comprising largely silt and clay with grain-size modes at or below the

410   sortable silt fraction (10–63 μm; Witus et al., 2014; Prothro et al., 2018; Jennings et al., 2022; Lepp et al., 2022). Fine silts in coastal settings (e.g., Manning et al., 2013) and glacial environments (e.g., Greco and Jaeger, 2020) behave cohesively and will form floccules with clays, which has important implications for plume migration and dispersal of MPDs into the marine environment. Silt floccules in the same size range as MPDs are experimentally shown to be stable in both freshwater and saline conditions at current speeds up to 25 cm s⁻¹ (Yawar and Schieber, 2017). In non-outburst style subglacial flow, aggregated

415   meltwater silts would have less exposed surface area onto which intergranular collisions could impart microtextures (Vos et al., 2014). This aggregate shielding effect could explain both the paucity of fluvial microtextures and retention of mechanical textures observed on MPDs, and is consistent with inferred episodic, low-magnitude drainage styles offshore eastern Thwaites Glacier (Lepp et al., 2022).

Alternatively, sluggish flow conditions and/or short transport distances may suffice to reduce grain relief and round

420   edges but be insufficient to impart abundant fluvial microtextures (Fig. 6). Microtexture studies on proglacial stream sediments find a positive correlation between transport distance and abundance of fluvial microtextures, but only after downstream transport distances between 3 km (Křížek et al., 2017) to at least 80 km (Sweet and Brannan, 2016) of downstream transport. For an evolving or transient subglacial drainage network through which flow is not constant or channelized, grains may be mobilized in suspension for only brief (i.e., sub-kilometer) distances before being deposited or entrained in basal ice via

425   supercooling, where alteration through intergranular collisions is minimal (Alley et al., 1997; Creyts and Clark, 2010; Alley et al., 2019). In the absence of supraglacial input to the bed, such continuous flow over several or tens of kilometers may not be sustained. Rather, grains comprising MPDs experience short "bursts" of energy and entrainment (i.e., during subglacial lake drainage events) or mobilization within a sluggish, lower flow regime (i.e., through water films or distributed drainage) wherein fluvial microtextures are not expected (Mahaney, 2002; Sweet and Brannan, 2016). Low flow regimes and modest grain

430   alteration in sediments from Thwaites Glacier is consistent with stratigraphic inferences from marine sediment cores collected from the Thwaites Eastern Ice Shelf (Lepp et al., 2022; Clark et al., 2023), while for other systems, like Pine Island Glacier and the eastern Ross Sea, some MPDs are interpreted to have rapidly accumulated through intensive, potentially catastrophic, subglacial drainage events (Lowe and Anderson, 2003; Kirshner et al., 2012; Witus et al., 2014; Prothro et al., 2018). MPD grains are significantly more regular and rounded than till and ice-proximal diamicton grains in these systems, which may be

435   the result of intensive, but short-lived, drainage events not recorded in the other glacial settings.

The most significant intra-site grain-shape alteration we see is between subglacial tills and MPDs from Ryder Glacier. In some locations, MPDs deposited during early to mid-Holocene retreat of Ryder Glacier are three to over five meters thick (O'Regan et al., 2021) indicating a highly active, well-connected subglacial drainage network coeval with elevated air temperatures and enhanced surface melt production (Levcavalier et al., 2017; McFarlin et al., 2018). Such a drainage

440   configuration and supply of meltwater to the ice bed would likely be capable of transporting water and sediments over long

(i.e., 10¹-10² km) distances. We interpret grain-shape alteration for this system to result from the combination of younger, less rounded grains in the till source (Fig. 4) and the input of supraglacial melt to the bed, as would be most common in temperate glacial conditions. While some glacial systems in West Antarctica show significant differences in grain solidity and circularity between grain populations, it is to a lesser magnitude than is observed in Ryder Glacier. We therefore infer that quantifiable

445   alteration of grains through meltwater action can be achieved through continuous sediment entrainment over long distances (i.e., many tens of kilometers) or through high-energy outburst-style flow, where a supraglacial supply of meltwater to the bed and younger, less reworked till grains can further enhance alteration. Conversely, the combination of mature till grains with poorly-developed channel networks, sluggish flow, and/or brief sediment transport distances may minimally or negligibly alter MPD grains from till sources. Results from Ryder Glacier suggest that a grain micromorphological approach may be valuable

450   in distinguishing temperate from polar conditions in the stratigraphic record.

4.4 On subglacial basins as reservoirs and subglacial lake drainage

Both model results (e.g., Carter et al., 2011) and satellite observations (Wingham et al., 2006; Fricker et al., 2007; Bowling et al., 2019; Hoffman et al., 2020) indicate subglacial water can be stored in, and actively transmitted between, subglacial basins, demonstrating connected subglacial plumbing that mirrors basin-channel systems preserved on deglaciated

455   continental shelves (e.g., Lowe and Anderson, 2003; Anderson and Fretwell, 2008; Kuhn et al., 2017; Simkins et al., 2017; Kirkham et al., 2019; Hogan et al., 2020). The importance of subglacial lakes as reservoirs of glacial melt and sediments have been evoked to explain discrepancies between annual production of basal melt and volume of water required to mobilize quantities of MPDs observed offshore (e.g., Witus et al., 2014; Schroeder et al., 2019; Lepp et al., 2022). For example, the distribution of ~120 km³ of silts deposited offshore of Pine Island Glacier is interpreted to have been sourced in part by high-

460   magnitude purging events of subglacial reservoirs of water and sediments (Witus et al., 2014). While our study includes samples from those deposits (Table A1) and results indicate significant alteration in MPD grain regularity from Pine Island Glacier tills (Fig. 4), neither our study nor the original found microtexture evidence expected from such high-energy sediment transport (Witus et al., 2014).

In general, the discrepancies between our grain-shape results and theories and observations of subglacial hydrologic

465   transport prompt a consideration of the extent to which sediments are cascaded (Siegfried et al., 2016; Malczyk et al., 2020; Livingstone et al., 2022) downstream along with water during subglacial lake drainage events. Beneath the contemporary West Antarctic Ice Sheet, flux of meltwater between subglacial lake basins has been indirectly observed over tens of meters beneath Thwaites Glacier (Hoffman et al., 2020; Malczyk et al., 2020). Channelized meltwater drainage under modern Thwaites Glacier is inferred to extend to the grounding line from 50 km upstream (Schroeder et al., 2013), yet MPD morphologies from this

470   region suggest discontinuous grain entrainment and nonturbulent flow (Fig. 4). In the Thor Iversenbanken region of the central Barents Sea, paleo-subglacial channels connecting basins are ~3-5 km in length (Esteves et al., 2022). While no Thor Iversenbanken samples were included in the microtexture analysis, the Z-scores indicate that grain shapes in till and MPDs are statistically the same (Table A2). This observation supports the importance of distance of subglacial hydrologic transport in

altering glacial silt morphology (Sweet and Brannan, 2016; Křížek et al., 2017). Drainage between East Antarctic subglacial
475   lakes is recorded over distances an order of magnitude higher (Wingham et al., 2006), implying that MPDs offshore the East
Antarctic Ice Sheet could show a higher abundance of glaciofluvial microtextures and/or shape alteration from till grains.
Recent insights from modern subglacial lake sediments recovered in the Siple Coast region of the Ross Sea drainage sector
suggest that silt-sized sediment can indeed be mobilized downstream between basins (Hodson et al., 2016) and cores from
subglacial lakes could represent a high-resolution record of drainage activity (Siegfried et al., 2023). We infer from the grain
480   micromorphology results presented here, however, that a linear, downstream transport of glacial silt through subglacial
plumbing networks enroute to the ocean is unlikely. Rather, the continued dominance of features indicating subglacial transport
through till deformation, with only minimal overprint of fluvial or meltwater features, suggests that while the final mode of
transport and grain sorting may be by subglacial meltwater, it is unlikely this sediment transport process dominates over large
areas or for extended periods of time (cf. Simkins et al., 2023).

485   **5 Conclusions**

Quantitative grain shape and microtexture analyses elucidate whether the shape of silt grains abundant in MPDs
record alteration by subglacial meltwater action from their till origins. By calculating grain shape metrics on thousands of
grains from six different glacial systems, we find that three-quarters of grains can be described by approximately one-quarter
of possible grain circularities, solidities, and eccentricities, providing evidence for efficient subglacial transport and erosive
490   processes operating at the catchment-wide scale. We find that MPD grains preserve surface textures diagnostic of sustained
stress and subglacial grinding but only modest evidence of fluvial transport. This indicates that glacial processes are responsible
for the unique grain-size production of MPDs and that, in general, alteration of grain micromorphology through hydrologic
transport is recorded more prominently by edge rounding and enhanced grain regularity than by imparting of surface textures.
We posit this may be due to an aggregate shielding effect and discontinuous transport distances and processes that are
495   insufficient to leave a pervasive microtextural mark. While regional geology, glacial history, and catchment size likely
influence variability in grain-shape distributions to a degree, these data suggest that the greatest grain-shape alteration occurs
when till sources are younger and subglacial meltwater flux is in part supplied by supraglacial input. Grain micromorphology
can be a valuable addition to traditional glacial and glaciomarine sediment analyses, in particular when subglacial drainage
networks are suspected to have been very active (i.e., draining of supraglacial melt), in determining whether the origin of
500   isolated silt laminae observed in sediment cores are of subglacial origin or result from melt-out from basal ice, and in
distinguishing polar from temperate glacial conditions within the stratigraphic record. Further, we encourage combined
empirical and experimental studies that incorporate grain micromorphology to quantifiably connect grain-shape alteration with
transport distance to better constrain realistic subglacial sediment transport pathways to the ocean.

505

Appendices

Table A1: Sample identification, coordinates, facies, water depth, associated glacial system or region, and reference for all samples used in this study. Relict glacial systems and regions that are no longer glaciated are italicized. ^ denotes meltwater plume deposits with no till counterpart. * indicates samples examined for microtexture analysis. Intervals indicate depth in the sediment core (with core top = 0) from which samples within the facies of interest were collected, and were chosen to avoid lithological boundaries. Negative elevation indicates water depth to core site, while positive elevation is used for reference materials. Diam. = diamicton.

Core ID	Interval *cm*	Latitude	Longitude	Elevation *m*	Facies	Glacial System/Region	Reference
Ryder19-6-GC	184-185	80.0095	-51.7408	-633	Meltwater	Ryder Glacier	O'Regan et al., 2021
Ryder19-7-PC	594-595	81.9518	-51.5878	-559	Meltwater	Ryder Glacier	O'Regan et al., 2021
Ryder19-7-PC *	878-879	81.9518	-51.5878	-559	Subglacial till	Ryder Glacier	O'Regan et al., 2021
Ryder19-8-PC *	920-921	81.8928	-51.1315	-238	Subglacial till	Ryder Glacier	O'Regan et al., 2021
Ryder19-9-PC *	622-623	81.8908	-50.9682	-274	Meltwater	Ryder Glacier	O'Regan et al., 2021
Ryder19-9PC *	830-831	81.8908	-50.9682	-274	Meltwater	Ryder Glacier	O'Regan et al., 2021
OD1507-18-GC ^	160-161	81.6266	-62.2989	-520	Meltwater	Petermann Glacier	Jennings et al., 2022
OD1507-31-PC ^	560-561	81.6106	-64.3522	-569	Meltwater	Nares Ice Stream	Jennings et al., 2022
CAGE-15-5-1221-GC	17-18	73.6098	34.6908	-253	Meltwater	*Thor Iversenbanken*	Esteves et al., 2022
CAGE-15-5-1221-GC	32-33	73.6098	34.6908	-253	Meltwater	*Thor Iversenbanken*	Esteves et al., 2022
CAGE-15-5-1221-GC	48-49	73.6098	34.6908	-253	Subglacial till	*Thor Iversenbanken*	Esteves et al., 2022
CAGE-15-5-1221-GC	61-62	73.6098	34.6908	-253	Subglacial till	*Thor Iversenbanken*	Esteves et al., 2022
CAGE-15-5-1222-GC	103-104	73.6173	34.6011	-310	Meltwater	*Thor Iversenbanken*	Esteves et al., 2022
CAGE-15-5-1222-GC	117-118	73.6173	34.6011	-310	Meltwater	*Thor Iversenbanken*	Esteves et al., 2022
CAGE-15-5-1222-GC	126-127	73.6173	34.6011	-310	Subglacial till	*Thor Iversenbanken*	Esteves et al., 2022
CAGE-15-5-1222-GC	133-134	73.6173	34.6011	-310	Subglacial till	*Thor Iversenbanken*	Esteves et al., 2022
JM-KA09-GC ^	341-342	74.8819	17.2035	-274	Meltwater	*Kveithola Ice Stream*	Rüther et al., 2012
DF85-115-PC	145-146	-68.4433	-70.7633	-726	Meltwater	*Marguerite Trough Ice Stream*	Kennedy & Anderson, 1989
DF85-115-PC	180-181	-68.4433	-70.7633	-726	Meltwater	*Marguerite Trough Ice Stream*	Kennedy & Anderson, 1989
DF85-115-PC	200-201	-68.4433	-70.7633	-726	Subglacial till	*Marguerite Trough Ice Stream*	Kennedy & Anderson, 1989
DF85-115-PC	205-206	-68.4433	-70.7633	-726	Subglacial till	*Marguerite Trough Ice Stream*	Kennedy & Anderson, 1989
DF85-116-PC	26-27	-68.4833	-70.6000	-650	Meltwater	*Marguerite Trough Ice Stream*	Kennedy & Anderson, 1989

Core ID	Interval *cm*	Latitude	Longitude	Elevation *m*	Facies	Glacial System/Region	Reference
DF85-116-PC	82-83	-68.4833	-70.6000	-650	Meltwater	*Marguerite Trough Ice Stream*	Kennedy & Anderson, 1989
DF85-116-PC	102-103	-68.4833	-70.6000	-650	Subglacial till	*Marguerite Trough Ice Stream*	Kennedy & Anderson, 1989
DF85-116-PC	143-144	-68.4833	-70.6000	-650	Subglacial till	*Marguerite Trough Ice Stream*	Kennedy & Anderson, 1989
OSO09-10 KC04	3-4	-72.6971	-107.1105	-729	Meltwater	Pine Island Glacier	Witus et al., 2014
OSO09-10 KC04 *	200-201	-72.6971	-107.1105	-729	Subglacial till	Pine Island Glacier	Witus et al., 2014
OSO09-10 KC18	30-31	-73.3835	-106.871	-894	Meltwater	Pine Island Glacier	Kirshner et al., 2012
OSO09-10 KC25	75-76	-73.2570	-107.1057	-838	Subglacial till	Pine Island Glacier	Kirshner et al., 2012
PIG-B	1-2	-75.0754	-100.432	-725	Meltwater	Pine Island Glacier	Smith et al., 2017
PIG-B	18-19	-75.0754	-100.432	-725	Ice- proximal diam.	Pine Island Glacier	Smith et al., 2017
PIG-B	80-81	-75.0754	-100.432	-725	Ice- proximal diam.	Pine Island Glacier	Smith et al., 2017
NBP20-02 KC26 *	70-72	-75.0215	-100.7513	-805	Ice- proximal diam.	Pine Island Glacier	This study
NBP19-02 KC04	170-172	-74.94	-106.18	-469	Ice- proximal diam.	Thwaites Glacier	Lepp et al., 2022
NBP19-02 KC13	10-12	-74.911	-106.953	-463	Meltwater	Thwaites Glacier	Clark et al., 2023
NBP19-02 JGC11	62-63	-75.058	-107.299	-752	Ice- proximal diam.	Thwaites Glacier	Clark et al., 2023
NBP19-02 KC15 *	80-82	-74.871	-106.333	-545	Meltwater	Thwaites Glacier	Clark et al., 2023
NBP19-02 JGC17	6-7	-74.887	-106.316	-507	Meltwater	Thwaites Glacier	Clark et al., 2023
NBP19-02 JGC17	106-107	-74.887	-106.316	-507	Ice- proximal diam.	Thwaites Glacier	Clark et al., 2023
NBP19-02 KC23	60-62	-75.07	-104.23	-677	Ice- proximal diam.	Thwaites Glacier	Lepp et al., 2022
NBP19-02 KC23	130-132	-75.07	-104.23	-677	Ice- proximal diam.	Thwaites Glacier	Lepp et al., 2022
NBP20-02 KC33	200-202	-74.64	-106.18	-397	Meltwater	Thwaites Glacier	Lepp et al., 2022
NBP20-02 KC67	50-52	-74.84	-104.46	-613	Meltwater	Thwaites Glacier	Lepp et al., 2022
NBP15-02 KC17	170-171	-75.874	179.666	-549	Meltwater	Western Ross Sea	Prothro et al., 2018
NBP15-02 KC19	115-116	-76.03	177.210	-455	Subglacial till	Western Ross Sea	Halberstadt et al., 2016
NBP15-02 KC19	145-146	-76.03	177.210	-455	Subglacial till	Western Ross Sea	Prothro et al., 2018
NBP15-02 KC22 *	115-116	-75.43	176.196	-354	Subglacial till	Western Ross Sea	Halberstadt et al., 2016
NBP15-02 KC22	120-121	-75.43	176.196	-354	Subglacial till	Western Ross Sea	Halberstadt et al., 2016
NBP15-02 KC24	79-80	-75.671	176.446	-450	Meltwater	Western Ross Sea	Simkins et al., 2017
Qaanaaq_1A	-	77.493	-69.242	372	Cryoconite	Qaanaaq Glacier	This study

Core ID	Interval *cm*	Latitude	Longitude	Elevation *m*	Facies	Glacial System/Region	Reference
Qaanaaq_2A	-	77.496	-69.229	456	Cryoconite	Qaanaaq Glacier	This study
Qaanaaq_3A	-	77.497	-69.200	556	Cryoconite	Qaanaaq Glacier	This study
SDM94	-	-81.643	-148.773	615	Basal ice debris	Siple Dome	This study
19-KP-H6	-	-75.215	-110.960	84	Fringe debris	Kay Peak, Pope Glacier	This study

Table A2: Results of two-type Z test and associated p-values performed on grain shape of meltwater plume deposit and till populations from each system. Z scores are absolute values. Shape metrics with statistically significantly different populations (Z > 3.0) are shown in bold.
515   Difference in means for those statistically significant metrics is presented with 95 % confidence interval calculated from 1,000 bootstrap replicates. Note the small values reflect both the range of the metric itself [0, 1] and supports the rejection of the null hypothesis that MPD and till sample populations are the same. Abbreviations of the glacial systems/regions are the same as in Figure 1.

		Ryder	TI	MTIS	PIG	TG	Ross Sea
Aspect Ratio	Z-Score	0.4131	0.01381	**5.8839**	2.9297	0.1616	0.3673
	p-value	0.680	0.581	$4.008e^{-9}$	$3.39e^{-3}$	0.872	0.713
	Difference in Means	-	-	$1.91e^{-2}\ ^{+6.31e^{-3}}_{-6.49e^{-3}}$	-	-	
Circularity	Z-Score	**11.313**	2.1265	0.6375	**3.7678**	0.5258	**6.4984**
	p-value	$< 2.2e^{-16}$	0.173	0.5238	$1.65e^{-4}$	0.599	$8.12e^{-11}$
	Difference in Means	$5.30e^{-2}\ ^{+9.92e^{-3}}_{-9.68e^{-3}}$	-	-	$1.60e^{-2}\ ^{+8.34e^{-3}}_{-8.66e^{-3}}$	-	$3.36e^{-2}\ ^{+1.06e^{-2}}_{-9.68e^{-3}}$
Eccentricity	Z-Score	0.6247	0.4847	**4.7231**	2.5914	0.0144	0.2989
	p-value	0.532	0.386	$2.32e^{-6}$	$9.56e^{-3}$	0.989	0.765
	Difference in Means	-	-	$3.95e^{-2}\ ^{+1.64e^{-2}}_{-9.52e^{-2}}$	-	-	
	Z-Score	**9.1276**	1.832	0.1234	**3.214**	1.056	**5.377**

Solidity	p-value	$< 2.2e^{-16}$	0.0570	0.9018	$1.31e^{-3}$	0.291	$7.57e^{-8}$
	Difference in Means	$3.34e^{-2}\ {}^{+7.13e^{-3}}_{-6.67e^{-3}}$	-	-	$1.05e^{-2}\ {}^{+6.52e^{-3}}_{-6.28e^{-3}}$	-	$2.02e^{-2}\ {}^{+6.88e^{-3}}_{-7.22e^{-3}}$

Data and Code availability

520   The datasets generated for this study, including the MATLAB script and results of grain-shape measurements, are available through the PANGAEA database (doi: PENDING). Additional data supporting the findings in this work can be requested from the corresponding author.

Author contribution

525   APL: conceptualization, data curation, formal analysis, investigation, methodology, project administration, software, visualization, writing – original draft. LEM: conceptualization, funding acquisition, methodology, project administration, resources, supervision, writing – review & editing. JBA: conceptualization, funding acquisition, writing – review & editing. MO, MCMW, ME: conceptualization, resources, writing – review & editing. JAS: funding acquisition, resources, writing – review & editing. LOP, EAP: resources, writing – review & editing. CDH, JSW: funding acquisition, writing – review & editing.

530 **Competing interests**

Co-author E.A. Podolskiy is a member of the editorial board of The Cryosphere, albeit for different subject areas than are most relevant to the content in this study. The peer-review process was guided by an independent editor, and the authors have no other competing interests to declare.

Acknowledgements

535   The authors acknowledge the captains, crews, and science parties who over the decades collected the dozens of cores sampled for this research. Funding for this research comes from a subcontract to the University of Virginia to LEM as part of the larger collaborative Thwaites Offshore Research grant (NSF OPP Grant 1738942 and Natural Environment Research Council grant nos. NE/S006664/1 and NE/S006672/1). We thank M. Esteves, V. Stanley, and the curatorial staff at the Oregon State University Marine and Geology Repository for their assistance with sample requests. D. Buskard and M. Prakash were

540   instrumental in developing the MATLAB script. The Quanta 650 SEM is housed in the Nanoscale Materials Characterization

Facility, and we thank the staff for providing the first author instrument training. Figures use the colorblind-friendly palette "Java" from the MetBrewer color package developed by B. R. Mills (https://github.com/BlakeRMills/MetBrewer). Data analysis and interpretation presented in this study was conducted at the University of Virginia in Charlottesville, Virginia. The University of Virginia was built by enslaved laborers on the unceded lands of the Monacan Nation, who have protected and
545 cultivated these lands for thousands of years. The authors acknowledge and respect their stewardship of the land, past, present, and future.

References

Alley, R. B., Blankenship, D. D., Bentley, C. R., and Rooney, S. T.: Deformation of till beneath ice stream B, West
550   Antarctica, Nature, 322, 57–59, doi: 10.1038/322057a0, 1986.
Alley, R.B., Cuffey, K.M., Evenson, E.B., Strasser, J.C., Lawson, D.E., and Larson, G.J.: How glaciers entrain and transport basal sediments: physical constraints, Quaternary Sci. Rev., 16, 1017-1038, doi: 10.1016/S0277-3791(97)00034-6, 1997.
Alley, R.B., Cuffey, K.M., and Zoet, L.K.: Glacial erosion: status and outlook, Ann. Glaciol., 60, 1-13, doi:
555   10.1017/aog.2019.38, 2019.
Anderson, J.B. and Fretwell, L.O.: Geomorphology of the onset area of a paleo-ice stream, Marguerite Bay, Antarctic Peninsula, Earth Surf. Proc. Land., 33, 503-512, doi: 10.1002/esp.1662, 2008.
Andreassen, K. and Winsborrow, M.: Signature of ice streaming in Bjørnøyrenna, Polar North Atlantic, through the Pleistocene and implications for ice-stream dynamics, Ann. Glaciol., 50, 17-26, doi:
560   10.3189/172756409789624238, 2009.
Blackman, D.K., Von Herzen, R.P., and Lawver, L.A.: Heat flow and tectonics in the Western Ross Sea, Antarctica, Vol. 5B9, 179-189, Earth Science Series, Circum-Pacific Council for Energy and Mineral Resources, 1987.
Boulton, G.S., Dobbie, K.E., and Zatsepin, S.: Sediment deformation beneath glaciers and its coupling to the subglacial hydraulic system, Quatern. Int., 86, 3-28, doi: 10.1016/S1040-6182(01)00048-9, 2001.
565 Bowling, J.S., Livingstone, S.J., Sole, A.J., and Chu, W.: Distribution and dynamics of Greenland subglacial lakes, Nat. Commun., 10, 2810, doi: 10.1038/s41467-019-10821-w, 2019.
Bjarnadóttir, L.R., Winsborrow, M.C.M., and Andreassen, K.: Deglaciation of the central Barents Sea, Quaternary Sci. Rev., 92, 208-226, doi: 10.1016/j.quascirev.2013.09.012, 2014.
Campaña, I., Benito-Calvo, A., Pérez-González, Bermúdez de Castro, J.M., and Carbonell, E.: Assessing automated image
570   analysis of sand grain shape to identify sedimentary facies, Gran Dolina archaeological site (Burgos, Spain), Sed. Geol., 346, 72-83, doi: 10.1016/j.sedgeo.2016.09.010, 2016.
Carter, S.P., Fricker, H.A., Blankenship, D.D., Johnson, J.V., Lipscomb, W.H., Price, S.F., and Young, D.A.: Modeling 5 years of subglacial lake activity in the MacAyeal Ice Stream (Antarctica) catchment through assimilation of ICESat laser altimetry, Ann. Glaciol., 57, 1098-1112, doi: 10.3189/002214311798843421, 2011.
575 Charpentier, I., Staszyc, A.B., Wellner, J.S., and Alejandro, V.: Quantifying grain shape with MorpheoLV: a case study using Holocene glacial marine sediments, EPJ Web of Conferences. Vol. 140. EDP Sciences, doi:10.1051/epjconf/201714014003, 2017.
Clark, R.W., Wellner, J.S., Hillenbrand, C.-D., Totten, R.L., Smith, J.A., Simkins, L.M., Larter, R.D., Hogan, K.A., Graha, A.G.C., Nitsche, F.O., Lehrmann, A.A., Lepp, A.P., Kirkham, J.D., Fitzgerald, V.T., Garcia-Barrera, G., Ehrmann,
580   W., and Wacker, L.: Synchronous retreat of Thwaites and Pine Island glaciers in response to external forcings in the pre-satellite era, P. Natl. Acad. Sci. USA (in press).
Cooper, A.K., Davey, F.J., and Behrendt, J.C.: The Antarctic Continental Margin: Geology and Geophysics of the Western Ross Sea, Vol. 5B9, 27-65, Earth Science Series, Circum-Pacific Council for Energy and Mineral Resources, 1987.

Cowan, E.A., Hillenbrand, C.-D., Hassler, L.E., and Ake, M.T.: Coarse-grained terrigenous sediment deposition on
585   continental rise drifts: a record of Plio-Pleistocene glaciation on the Antarctic Peninsula, Palaeogeogr. Palaeocl.,
           265, 275-291, doi: 10.1016/j.palaeo.2008.03.010, 2008.
Cowan, E.A., Christoffersen, P., and Powell, R.D.: Sedimentological signature of a deformable bed preserved beneath an ice
           stream in a late Pleistocene glacial sequence, Ross Sea, Antarctica, J. Sediment. Res., 82, 270-282, doi:
           10.2110/jsr.2012.25, 2012.
590 Creyts, T.T. and Clarke, G.K.C.: Hydraulics of subglacial supercooling: theory and simulations for clear water flows, J.
           Geophys. Res.-Earth, 115, F03021, doi: 10.1029/2009JF001417, 2010.
Crompton, J.W., Flowers, G.E., and Dyck, B.: Characterization of glacial silt and clay using automated mineralogy, Ann.
           Glaciol., 60, 49-65, doi: 10.1017/aog.2019.45, 2019.
Damiani, T.M., Jordan, T.A., Ferraccioli, F., Young, D.A., and Blankenship, D.D.: Variable crustal thickness beneath
595   Thwaites Glacier revealed from airborne gravimetry, possible implications for geothermal heat flux in West
           Antarctica, Earth Planet. Sc. Lett., 407, 109-122, doi: 10.1016/j.espl.2014.09.023, 2014.
Domack, E.W., Jacobson, E.K., Shipp, S., and Anderson, J.B.: Late Pleistocene-Holocene retreat of the west Antarctic ice
           sheet system in the Ross Sea: Part 2 – sedimentologic and stratigraphic signature, Geol. Soc. Am. Bull., 111, 1517-
           1536, 1999.
600 Dreimanis, A., and Vagners, U.J: Bimodal distribution of rock and mineral fragments in basal tills, Glacial Till: An
           Interdisciplinary Study, edited by: Legget, R.F., Royal Society of Canada, Special Publication, 12, 237-250, 1971.
Dreimanis, A., and Vagners, U.J.: The effect of lithology upon texture of till, Research methods in Pleistocene
           geomorphology, 66-82, 1972.
Dziadek, R., Ferraccioli, F., and Gohl, K.: High geothermal heat flow beneath Thwaites Glacier in West Antarctica inferred
605   from aeromagnetic data, Nat. Commun. Earth Environ., 162, doi: 10.1038/s43247-012-00242-3, 2021.
Ehrmann, W., Hillenbrand, C.-D., Smith, J.A., Graham, A.G.C., Kuhn, G., and Larter, R.D.: Provenance changes between
           recent and glacial-time sediments in the Amundsen Sea embayment, West Antarctica: clay mineral assemblage
           evidence, Antarct. Sci., 23, 471-486, doi: 10.1017/S0954102011000320, 2011.
Esteves, M., Bjarnadóttir, L.R., Winsborrow, M.C.M., Shackleton, C.S., and Andreassen, K.: Retreat patterns and dynamics
610   of the Sentralbankrenna glacial system, central Barents Sea, Quaternary Sci. Rev., 169, 131-147, doi:
           10.1016/j.quascirev.2017.06.004, 2017.
Esteves, M., Rüther, D., Winsborrow, M. C. M., Livingstone, S. J., Shackleton, C. S., and Andreassen, K.: An
           interconnected palaeo-subglacial lake system in the central Barents Sea, EarthArxiv [ArXiv pre-print],
           doi:10.31223/X58934, 2022.
615 Evans D.J.A., Phillips, E.R., Hiemstra, J.F., and Auton, C.A.: Subglacial till: Formation, sedimentary characteristics and
           classification, Earth-Sci. Rev, 78, 115-176, doi: 10.1016/j.earscirev.2006.04.001, 2006.
Evans, J., Pudsey, C.J., Ó Cofaigh, C., Morris, P., and Domack, E.: Late Quaternary glacial history, flow dynamics, and
           sedimentation along the eastern margin of the Antarctic Peninsula Ice Sheet, Quaternary Sci. Rev., 24, 741-774,
           doi: 10.1016/j.quascirev.2004.10.007, 2005.
620 Flowers, G.E.: Hydrology and the future of the Greenland Ice Sheet, Nat. Commun., 9, 2729, doi: 10.1038/s41467-018-
           05002-0, 2018.
Fricker, H.A., Scambos, T., Bindschadler, R., and Padman, L.: An active subglacial water system in West Antarctica mapped
           from space, Science, 315, 1544-1548, doi: 10.1126/science.1136897, 2007.
Gilbert, E., and Kittel, C.: Surface melt and runoff on Antarctic ice shelves at 1.5 °C, 2 °C, and 4 °C of future warming,
625   Geophys. Res. Lett., 48, e2020GL091733, doi: 10.1029/2020GL091733, 2021.
Greco, N., and Jaeger, J.M.: Modeling Mud: Flocs as Global Meltwater Indicators in Ice-Proximal Glacimarine Sediments,
           AGU Fall Meeting Abstracts, 2020, EP001-0014, 2020.
Greenwood, S. L., Gyllencreutz, R., Jakobsson, M., and Anderson, J. B.: Ice-flow switching and East/West Antarctic Ice
           Sheet roles in glaciation of the western Ross Sea, Geol. Soc. Am. Bull., 124, 1736–1749, doi:10.1130/B30643.1,
630   2012.
Greenwood, S.L., Clason, C.C., Helanow, C., and Margold, M.: Theoretical, contemporary observational and palaeo-
           perspectives on ice sheet hydrology: Processes and products, Earth Sci. Rev., 15, 1-27,
           doi:10.1016/j.earscirev.2016.01.010, 2016.

Greenwood, S. L., Simkins, L. M., Winsborrow, M. C. and Bjarnadóttir, L. R. Exceptions to bed-controlled ice sheet flow
and retreat from glaciated continental margins worldwide. Sci. Adv. 7, doi:10.1126/sciadv.abb6291, 2021.

Gustafson, C.D., Key, K., Siegfried, M.R., Winberry, J.P., Fricker, H.A., Venturelli, R.A., and Michaud, A.B.: A dynamic
saline groundwater system mapped beneath an Antarctic ice stream, Science, 376, 640-644, doi:
10.1126/science.abm3301, 2022.

Halberstadt, A.R.W, Simkins, L., Greenwood, S., and Anderson, J., Past ice-sheet behaviour: Retreat scenarios and changing
controls in the Ross Sea, Antarctica, Cryosphere, 10, 1003-1020, doi: 10.5194/tc-10-1003-2016, 2016.

Halberstadt, A.R.W., Simkins, L.M., Anderson, J.B., Prothro, L.O., and Bart, P.J.: Characteristics of the deforming bed: till
properties on the deglaciated Antarctic continental shelf. J. Glaciol., 64, 1014-1027, doi: 10.1017/jog.2018.92,
2018.

Haldorsen, S.: Grain-size distribution of subglacial till and its relation to glacial crushing and abrasion, Boreas, 10, 91-105,
doi: 10.1111/j.1502-3885.1981.tb00472.x, 1981.

Hart, J.K.: Athabasca Glacier, Canada – a field example of subglacial ice and till erosion? Earth Surf. Proc. Land., 31, 65-80,
doi: 10.1002/esp.1233, 2006.

Hillenbrand, C.-D., Grobe, H., Diekmann, B., Kuhn, G., and Fütterer, D.K.: Distribution of clay minerals and proxies for
productivity in surface sediments of the Bellingshausen and Amundsen seas (West Antarctica) – relation to modern
environmental conditions, Mar. Geol., 193, 253-271, doi: 10.1016/S0025-3227(02)00659-X, 2003.

Hillenbrand, C.-D., Kuhn, G., Smith, J.A., Gohl, K., Graham, A.G.C., Larter, R.D., Klages, J.P., Downey, R., Moreton, S.G.,
Forwick,M., and Vaughan, D.G.: Grounding-line retreat of the West Antarctic Ice Sheet from inner Pine Island Bay,
Geology, 41, 35-38, doi: 10.1130/G33469.1, 2013.

Hoffman, A.O., Christianson, K., Shapero, D., Smith, B.E., and Joughin, I.: Brief Communication: Heterogenous thinning
and subglacial lake activity on Thwaites Glacier, West Antarctica, Cryosphere, 14, 4603-4609, doi: 10.5194/tc-14-
4603-2020, 2020.

Hogan, K.A., Jakobsson, M., Mayer, L., Reilly, B.T., Jennings, A.E., Stoner, J.S., Nielsen, T., Andresen, K.J., Nørmark, E.,
Heirman, K.A., Kamla, E., Jerram, K., Stranne, C., and Mix, A.: Glacial sedimentation, fluxes, and erosion rates
associated with ice retreat in Petermann Fjord and Nares Strait, north-west Greenland, Cryosphere, 14, 261-286,
doi: 10.5194/tc-14-261-2020, 2020.

Hogan, K.A., Arnold, N.S., Larter, R.D., Kirkham, J.D., Noormets, R., Ó Cofaigh, C., Golledge, N.R., and Dowdeswell,
J.A.: Subglacial water flow over an Antarctic palaeo-ice stream bed, , J. Geophys. Res.-Earth, 127, e2021JF006442,
doi: 10.1029/2021JF006442, 2022.

Immonen, N.: Surface microtextures of ice-rafted quartz grains revealing glacial ice in the Cenozoic Arctic, Palaeogeogr.
Palaeocl., 374, 293-302, doi: 10.1016/j.palaeo.2013.02.003, 2013.

Iverson, N.R., Hooyer, T.S., and Hooke, R.L.: A laboratory study of sediment deformation: stress heterogeneity and grain-
size evolution, Ann. Glaciol., 22, 167-175, doi: 10.3189/1996AoG22-1-167-175, 1996.

Iverson, N.R.: Shear resistance and continuity of subglacial till: hydrology rules, J. Glaciol., 56, 1104-1114, doi:
10.3189/002214311796406220, 2010.

Iverson, N.R., McCracken, R.G., Zoet, L.K., Benediktsson, Í. Ö., Schomacker, A., Johnson, M.D., and Woodard, J.: A
theoretical model of drumlin formation based on observations at Múlajökull, Iceland, J. Geophys. Res.-Earth, 122,
2302-2323, doi: 10.1002/2017JF004354, 2017.

Jakobsson, M., Hogan, K.A., Mayer, L.A., Mix, A., Jennings, A., Stoner, J., Eriksson, B., Jerram, K., Mohammad, R.,
Pearce, C., Reilly, B., and Stranne, C.: The Holocene retreat dynamics and stability of Petermann Glacier in
northwest Greenland, Nat. Commun., 9, 2104, doi: 10.1038/s41467-018-04573-2, 2018.

Jennings, A., Reilly, B., Andrews, J., Hogan, K., Walczak, M., Jakobsson, M., Stoner, J., Mix, A., Nicholls, K.W., O'Regan,
M., Prins, M.A., and Troelstra, S.R.: Modern and early Holocene ice shelf sediment facies from Petermann Fjord
and northern Nares Strait, northwest Greenland, Quaternary Sci. Rev., 283, 107460, doi:
10.1016/j.quascirev.2022.107460, 2022.

Kennedy, D.S. and Anderson, J.B.: Glacial-marine sedimentation and Quaternary glacial history of Marguerite Bay,
Antarctic Peninsula, Quaternary Res., 31, 255-276, doi: 10.1016/0033-5894(89)90008-2, 1989.

Kilfeather, A.A., Ó Cofaigh, C., Lloyd, J.M., Dowdeswell, J.A., Xu, S., and Moreton, S.G.: Ice-stream retreat and ice-shelf history in Marguerite Trough, Antarctic Peninsula: Sedimentological and foraminiferal signatures, Geol. Soc. Am. Bull., 123, 997-1015, doi: 10.1130/B30282.1, 2011.

685 Kirkham, J.D., Hogan, K.A., Larter, R.D., Arnold, N.S., Nitsche, F.O., Goleldge, N.R., and Dowdeswell, J.A.: Past water flow beneath Pine Island and Thwaites glaciers, West Antarctica, Cryosphere, 13, 1959-1981, doi:10.5194/tc-13-1959-2019, 2019.

Kirkham, J.D., Hogan, K.A., Larter, R.D., Arnold, N.S., Nitsche, F.O., Kuhn, G., Gohl, K., Anderson, J.B., and Dowdeswell, J.A.: Morphometry of bedrock meltwater channels on Antarctic inner continental shelves: Implications for channel 690 development and subglacial hydrology, Geomorphology, 370, 107369, doi: 10.1016/j.geomorph.2020.107369, 2020.

Kirshner, A.E., Anderson, J.B., Jakobsson, M., O'Regan, M., Majewski, W., and Nitsche, F.O.: Post-LGM deglaciation in Pine Island Bay, West Antarctica, Quaternary Sci. Rev., 38, 11-26, doi: 10.1016/j.quascirev.2012.01.017, 2012.

Křížek, M., Krbcová, K., Mida, P., and Hanáček, M.: Micromorphological changes as an indicator of the transition from 695 glacial to glaciofluvial quartz grains: Evidence from Svalbard, Sediment. Geol., 358, 35-43, doi:10.1016/j.sedgeo.2017.06.010, 2017.

Kuhn, G., Hillenbrand, C.-D., Kasten, S., Smith, J.A., Nitsche, F.O., Frederichs, T., Wiers, S., Ehrmann, W., Klages, J.P., and Mogollon, J.M.: Evidence for a palaeo-subglacial lake on the Antarctic continental shelf, Nat. Commun., 8, 15591, doi: 10.1038/ncomms15591, 2017.

700 Larter, R.D., Anderson, J.B., Graham, A.G.C., Gohl, K., Hillenbrand, C.-D., Jakobsson, M., Johnson, J.S., Kuhn, G., Nitsche, F.O., Smith, J.A., Witus, A.E., Bentley, M.J., Dowdeswell, J.A., Ehrmann, W., Klages, J.P., Lindow, J., Ó Cofaigh, C., and Spiegel, C.: Reconstruction of changes in the Amundsen Sea and Bellingshausen Sea sector of the West Antarctic Ice Sheet since the Last Glacial Maximum, Quaternary Sci. Rev., 100, 55-86, doi: 10.1016/j.quascirev.2013.10.016, 2014.

705 Lecavalier, B.S., Fisher, D.A., Milne, G.A., Vinther, B.M., Tarasov, L., Huybrechts, P., Lacelle, D., Main, B., Zheng, J., Bourgeois, J., and Dyke, A.S.: High Arctic Holocene temperature record from the Agassiz ice cap and Greenland ice sheet evolution, P. Natl. Acad. Sci. USA, 114, 5952-5957, doi: 10.1073/pnas.1616287114, 2017.

Lenaerts, J.T.M., Vizcaino, M., Fyke, J., van Kampenhout, L., and van den Broeke, M.R.: Present-day and future Antarctic ice sheet climate and surface mass balance in the Community Earth System Model, Clim. Dynam., 47, 1367-1381, 710 doi: 10.1007/s00382-015-2907-4, 2016.

Lepp, A.P., Simkins, L.M., Anderson, J.B., Clark, R.W., Wellner, J.S., Hillenbrand, C.-D., Smith, J.A., Lehrmann, A.A., Totten, R., Larter, R.D., Hogan, K.A., Nitsche, F.O., Graham, A.G.C., and Wacker, L.: Sedimentary signatures of persistent subglacial meltwater drainage from Thwaites Glacier, Antarctica, Front. Earth Sci., 10:863200, doi: 10.3389/feart.2022.863200, 2022.

715 Lešić, N.-M., Streuff, K.T., Bohrmann, G., and Kuhn, G.: Glacimarine sediments from outer Drygalski Trough, sub-Antarctic South Georgia – evidence for extensive glaciation during the Last Glacial Maximum, Quaternary Sci. Rev., 292, 107657, doi: 10.1016/j.quascirev.2022.107657, 2022.

Licht, K.J., Lederer, J.R., and Swope, R.J.: Provenance of LGM glacial till (sand fraction) across the Ross embayment, Antarctica, Quaternary Sci. Rev., 24, 1499-1520, doi: 10.1016/j.quascirev.2004.10.017, 2005.

720 Livingstone, S.J., Ó Cofaigh, C., Stokes, C.R., Hillenbrand, C.-D., Vieli, A., and Jamieson, S.S.R.: Glacial geomorphology of Marguerite Bay Palaeo-Ice stream, western Antarctic Peninsula, J. Maps, 9, 558-572, doi: 10.1080/17445647.2013.829411, 2013.

Livingstone, S.J., Li, Y., Rutishauser, A., Sanderson, R.J., Winter, K., Mikucki, J.A., Björnsson, H., Bowling, J.S., Chu, W., Dow, C.F., Fricker, H.A., McMillan, M., Ng, F.S.L., Ross, N., Sieger, M.J., Siegfried, M., and Sole, A.J.: 725 Subglacial lakes and their changing role in a warming climate, Nat. Rev. Earth Environ., 3, 106-124, doi: 10.1038/s43017-021-00246-9, 2022.

Livsey, D.N., Simms, A.R., Clary, W.G., Wellner, J.S., Anderson, J.B., and Chandler, J.P.: Fourier grain-shape analysis of Antarctic marine core: the relative influence of provenance and glacial activity on grain shape, J. Sediment. Res.,

Mahaney, W.C.: Atlas of sand grain surface textures and applications, Oxford University Press, USA, 2002.

730 Malczyk, G., Gourmelen, N., Goldberg, D., Wuite, J., and Nagler, T.: Repeat subglacial lake drainage and filling beneath Thwaites Glacier, Geophys. Res. Lett., 47, e2020GL089658, doi: 10.1029/2020GL089658, 2020.

Manning, A.J., Spearman, J.R., Whitehouse, R.J.S., Pidduck, E.L., Baugh, J.V., and Spencer, K.L.: Flocculation Dynamics of Mud: San Mixed Suspensions, in: Sediment transport processes and their modelling applications, edited by: Manning, A.J., InTech, Rijeka, Croatia, 119-125, doi:10.5772/55233, 2013.

735 Marsaglia, K., Milliken, K., and Doran, L.: IODP digital reference for smear slide analysis of marine mud. Part 1: Methodology and atlas of siliciclastic and volcanogenic components, IODP Technical Note 1, doi: 10.2204/iodp.tn.1.2013, 2013.

McFarlin, J.M., Axford, Y., Osburn M.R., Kelly, M.A., Osterberg, E.C., and Farnsworth, L.B.: Pronounced summer warming in northwest Greenland during the Holocene and Last Interglacial, P. Natl. Acad. Sci. USA, 201720420, 740 doi: 10.1073/pnas.1720420115, 2018.

Menzies, J.: Strain pathways, till internal architecture and microstructures-perspectives on a general kinematic model – a 'blueprint' for till development, Quaternary Sci. Rev., 50, 105-124, doi: 10.1016/j.quascirev.2012.07.012, 2012.

Meyer, C.R., Robel, A.A., and Rempel, A.W.: Frozen fringe explains sediment freeze-on during Heinrich events, Earth Plan. Sci. Lett., 524, 115725, doi: 10.1016/j.eosl.2019/115725, 2019.

745 Munoz, Y.P. and Wellner, J.S.: Seafloor geomorphology of western Antarctic Peninsula bays: a signature of ice flow behavior, Cryosphere, 12, 205-225, doi: 10.5194/tc-12-205-2018, 2018.

Muto, A., Peters, L.E., Gohl, K., Sasgen, I., Alley, R.B., Anandakrishnan, S., and Riverman, K.L.: Subglacial bathymetry and sediment distribution beneath Pine Island Glacier ice shelf modeled using aerogravity and in situ geophysical data: new results, Earth Planet. Sc. Lett., 443, 63-75, doi: 10.1016/j.epsl.2015.10.037, 2016.

750 Nitsche, F.O., Gohl, K., Larter, R.D., Hillenbrand, C.D., Kuhn, G., Smith, J.A., Jacobs, S., Anderson, J.B., and Jakobsson, M.: Paleo ice flow and subglacial meltwater dynamics in Pine Island Bay, West Antarctica, Cryosphere, 7, 249– 262, doi:10.5194/tc-7-249-2013, 2013.

Ó Cofaigh, C. and Dowdeswell, J.A.: Laminated sediments in glacimarine environments: diagnostic criteria for their interpretation, Quaternary Sci. Rev., 20, 1411-1436, doi: 10.1016/S0277-3791(00)00177-3, 2001.

755 Ó Cofaigh, C., Dowdeswell, J.A., Allen, C.S., Hiemstra, J.F., Pudsey, C.J., Evans, J., and Evans, D.J.A.: Flow dynamics and till genesis associated with a marine-based Antarctic palaeo-ice stream, Quaternary Sci. Rev., 24, 709-740, doi: 10.1016/j.quascirev.2004.10.006, 2005.

Ó Cofaigh, C., Davies, B.J., Livingstone, S.J., Smith, J.A., Johnson, J.S., Hocking, E.P., Hodgson, D.A., Anderson, J.B., Bentley, M.J., Canals, M., Domack, E., Dowdeswell, J.A., Evans, J., Glasser, N.F., Hillenbrand, C.-D., Larter, R.D., 760 Roberts, S.J., and Simms, A.R.: Reconstruction of ice-sheet changes in the Antarctic Peninsula since the Last Glacial Maximum, Quaternary Sci. Rev., 100, 87-100, doi: 10.1016/j.quascirev.2014.06.023, 2014.

Oakey, R.J., Green, M., Carling, P.A., Lee, M.W.E., Sear, D.A., and Warburton, J.: Grain-shape analysis – a new method for determining representative particle shapes for populations of natural grains, J. Sediment. Res., 75, 1065-1073, doi: 10.2110/jsr.2005.079, 2005.

765 O'Regan, M., Cronin, T.M., Reilly, B., Alstrup, A.K.O., Gemery, L., Golub, A., Mayer, L.A., Morlighem, M., Moros, M., Munk, O.L., Nilsson, J., Pearce, C., Detlef, H., Stranne, C., Vermassen, F., West, G., and Jakobsson, M.: The Holocene dynamics of Ryder Glacier and ice tongue in north Greenland, Cryosphere, 15, 4073–4097, doi:10.5194/tc-15-4073-2021, 2021.

Passchier, S., Hansen, M.A., and Rosenberg, J.: Quartz grain microtextures illuminate Pliocene periglacial sand fluxes on the 770 Antarctic continental margin, the Depositional Record, 7, 564-581, doi: 10.1002/dep2.157, 2021.

Prothro, L.O., Simkins, L.M., Majewski, W., and Anderson, J.B.: Glacial retreat patterns and processes determined from integrated sedimentology and geomorphology records. Mar. Geol., 395, 104-119, doi:10.1016/j.margeo.2017.09.012, 2018.

Reinardy, B.T.I., Hiemstra, J.F., Murray, T., Hillenbrand, C.-D., and Larter, R.D.: Till genesis at the bed of an Antarctic 775 Peninsula palaeo-ice stream as indicated by micromorphological analysis, Boreas, 40, 498-517, doi: 10.1111/j.1502-3885.2010.00199.x, 2011.

Rempel, A.W.: A theory for ice-till interactions and sediment entrainment beneath glaciers, J. Geophys. Res.-Earth, 113, F01013, doi: 10.1029/2007/JF000870, 2008.

Rilling, S., Mukasa, S., Wilson, T., Lawver, L., and Hall, C.: New determinations of 40Ar/39 780 Ar isotopic ages and flow volumes for Cenozoic volcanism in the Terror Rift, Ross Sea, Antarctica, J. Geophys. Res. 114, B12207, doi:10.1029/2009JB006303, 2009.

Robinson, D.E., Menzies, J., Wellner, J.S., and Clark, R.W.: Subglacial sediment deformation in the Ross Sea, Antarctica, Quaternary Sci. Adv., 4, 100029, doi:10.1016/j.qsa.2021.100029, 2021.

Rose, K.C., and Hart, J.K.: Subglacial comminution in the deforming bed: inferences from SEM analysis, Sediment. Geol., 203, 87-97, doi: 10.1016/j.sedgeo.2007.11.003, 2008.

Roseby, Z.A., Smith, J.A., Hillenbrand, C.-D., Cartigny, M.J.B., Rosenheim, B.E., Hogan, K.A., Allen, C.S., Leventer, A., Kuhn, G., Ehrmann, W., and Larter, R.D.: History of Anvers-Hugo Trough, western Antarctic Peninsula shelf, since the Last Glacial Maximum. Part I: Deglacial history based on new sedimentological and chronological data, Quaternary Sci. Rev., 291, 107590, doi: 10.1016/j.quascirev.2022.107590, 2022.

Rüther, D.C., Bjarnadóttir, L.R., Junttila, J., Husum, K., Rasmussen, T.L., Lucchi, R.G., and Andreassen, K.: Pattern and timing of the northwestern Barents Sea Ice Sheet deglaciation and indications of episodic Holocene deposition, Boreas, 41, 494-512, doi: 10.1111/j.1502-3885.2011.00244.x, 2012.

Schroeder, D.M., Blankenship, D.D., and Young, D.A.: Evidence for a water system transition beneath Thwaites Glacier, West Antarctica, P. Natl. Acad. Sci. USA, 110, 12225-12228, doi:10.1073/pnas.1302828110, 2013.

Schroeder, D.M., Blankenship, D.D., Young, D.A., Witus, A.E., and Anderson, J.B.: Airborne radar sounding evidence for deformable sediments and outcropping bedrock beneath Thwaites Glacier, West Antarctica, Geophys. Res. Lett, 41, 7200, 7208, doi: 10.1002/2014GL061645, 2014.

Schroeder, D.M., MacKie, E.J., Creyts, T.T., and Anderson, J.B.: A subglacial hydrologic drainage hypothesis for silt sorting and deposition during retreat in Pine Island Bay, Ann. Glaciol., 60, 14–20, doi:10.1017/aog.2019.44, 2019.

Siegfried, M.R., Fricker, H.A., Carter, S.P., and Tulaczyk, S.: Episodic ice velocity fluctuations triggered by a subglacial flood in West Antarctica, Geophys. Res. Lett., 43, 2640-2648, doi: 10.1002/2016GL067758, 2016.

Siegfried, M.R., Venturelli, R.A., Patterson, M.O., Arnuk, W., Campbell, T.D., Gustafson, C.D., Michaud, A.B., Galton-Fenzi, B.K., Hausner, M.B., Holzschuh, S.N., Huber, B., Manoff, K.D., Schroeder, D.M., Summers, P.T., Tyler, S., Carter, S.P., Fricker, H.A., Harwood, D.M., Leventer, A., Rosenheim, B.E., Skidmore, M.L., Priscu, J.C., and the SALSA Science Team: The life and death of a subglacial lake in West Antarctica, Geology, 51, 434-438, doi: 10.1130/G50995.1, 2023.

Simkins, L.M., Anderson, J.B., Prothro, L.O., Halberstadt, A.R.W., Stearns, L.A., Pollard, D., and DeConto, R.M.: Anatomy of a meltwater drainage system beneath the ancestral East Antarctic ice sheet, Nat. Geosci., 10, 691-697, doi:10.1038/ngeo3012, 2017.

Simkins, L.M., Greenwood, S.L., and Anderson, J.B.: Diagnosing ice sheet grounding line stability from landform morphology, Cryosphere, 12, 2707-2726, doi:10.5194/tc-12-2707-2018, 2018.

Simkins, L.M., Greenwood, S.L., Winsborrow, M.C.M., Bjarnadóttir, L.R., and Lepp, A.P.: Advances in understanding subglacial meltwater drainage from past ice sheets, Ann. Glaciol., 1-5, doi: 10.1017/aog.2023.16, 2023.

Simões Pereira, P., van de Flierdt, T., Hemming, S.R., Frederichs, T., Hammond, S.J., Brachfeld, S., Doherty, C., Kuhn, G., Smith, J.A., Klages, J.P., and Hillenbrand, C.-D.: The geochemical and mineralogical fingerprint of West Antarctica's weak underbelly: Pine Island and Thwaites glaciers, Chem. Geol., 550, 119649, doi: 10.1016/j.chemgeo.2020.119649, 2020.

Smith, A.M., Jordan, T.A., Ferraccioli, F., and Bingham, R.G.: Influence of subglacial conditions on ice stream dynamics: seismic and potential field data from Pine Island Glacier, West Antarctica, J. Geophys. Res.-Earth, 118, 1471-1482, doi: 10.1029/2012JB009582, 2013.

Smith, J.A., Anderson, T.J., Shortt, M., Gaffney, A.M., Truffer, M., Stanton, T.P., Bindschadler, R., Dutrieux, P., Jenkins, A., Hillenbrand, C.-D., Ehrmann, W., Corr, H.F.J., Farley, N., Crowhurst, S., and Vaughan, D.G.: Sub-ice-shelf sediments record history of twentieth-century retreat of Pine Island Glacier, Nature, 541, 77-80, doi: 10.1038/nature20136, 2017.

St. John, K., Passchier, S., Tantillo, B., Darby, D., and Kearns, L.: Microtextures of modern sea-ice-rafted sediment and implications for paleo-sea-ice reconstructions, Ann. Glaciol., 56, 83-93, doi: 10.3189/2015AoG69A586, 2015.

Stearns, L. A., Smith, B. E., and Hamilton, G. S.:Increased flow speed on a large East Antarctic outlet glacier caused by subglacial floods, Nat. Geosci. Letters, 1, 827-831, doi:10.1038/ngeo356, 2008.

Streuff, K., Ó Cofaigh, C., Hogan, K., Jennings, A., Lloyd, J.M., Noormets, R., Nielsen, T., Juijpers, A., Dowdeswell, J.A., and Weinrebe, W.: Seafloor geomorphology and glacimarine sedimentation associated with fast-flowing ice sheet

outlet glaciers in Disko Bay, West Greenland, Quaternary Sci. Rev., 169, 206-230 doi: 10.1016/j.quascirev.2017.05.021, 2017.

Sweet, D.E., and Brannan, D.K.: Proportion of glacially to fluvially induced quartz grain microtextures along the Chitina River, SE Alaska, U.S.A., J. Sediment. Res., 86, 749-761, doi: 10.2110/jsr.2016.49, 2016.

835 Trusel, L.D., Frey, K.E., Das, S.B., Karnauskas, K.B., Munneke, P.K., van Meijgaard, E., and van den Broeke, M.R.: Divergent trajectories of Antarctic surface melt under two twenty-first-century climate scenarios, Nat. Geosci., 8, 927-932, doi: 10.1038/ngeo2563, 2015.

van Hateren, J.A., van Buuren, U., Arens, S.M., van Balen, R.T., and Prins, M.A.: Identifying sediment transport mechanisms from grain size-shape distributions, applied to aeolian sediments, Earth Surf. Dynam., 8, 527-553,
840 doi:10.5194/esurf-8-527-2020, 2020.

Vos, K.,Vandenberghe, N., and Elsen, J.: Surface textural analysis of quartz grains by scanning electron microscopy (SEM): From sample preparation to environmental interpretation, Earth-Sci. Rev., 128, 193-104, doi:10.1016/j.earscirev.2013.10.013, 2014.

Yawar, Z. and Schieber, J.: On the origin of silt laminae in laminated shales, Sediment. Geol., 360, 22-34,
845 doi:10.1016/j.sedgeo.2017.09.001, 2017.

Wellner, J.S., Anderson, J.B., Ehrmann, W., Weaver, F.M., Kirshner, A., Livsey, D., and Simms, A.R.: History of an Evolving Ice Sheet as Recorded in SHALDRIL Cores From the Northwestern Weddell Sea, Antarctica, in: Tectonic, Climatic, and Cryospheric Evolution of the Antarctic Peninsula, American Geophysical Union, Washington, DC, USA, 131-151, doi: 10.1029/2010SP001047, 2011.

850 Wingham, D.J., Siegert, M.J., Shepherd, A., and Muir, A.S.: Rapid discharge connects Antarctic subglacial lakes, Nature, 440, 1033-1036, doi: 10.1038/nature04660, 2006.

Winsborrow, M.C.M., Andreassen, K., Corner, G.D., and Laberg, J.S.: Deglaciation of a marine-based ice sheet: Late Weichselian palaeo-ice dynamics and retreat in the southern Barents Sea reconstructed from onshore and offshore glacial geomorphology, Quaternary Sci. Rev., 29, 424-442, doi: 10.1016/j.quascirev.2009.10.001, 2010.

855 Witus, A.E., Branecky, C.M., Anderson, J.B., Szczucinski, W., Schroeder, D.M., Blankenship, D.D., and Jakobsson, M.: Meltwater intensive retreat in polar environments and investigation of associated sediments: example from Pine Island Bay, West Antarctica, Quaternary Sci. Rev., 85, 99–118, doi:10.1016/j.quascirev.2013.11.021, 2014.